Numerical analysis of air-water-heat flow in unsaturated soil: Is it necessary to consider airflow in land surface models?

Yijian Zeng,[1,2] Zhongbo Su,[2] Li Wan,[1] and Jun Wen[3]

Received 21 February 2011; revised 5 August 2011; accepted 5 August 2011; published 20 October 2011.

[1] From a subsurface physical point of view, this paper discusses the necessity of considering the two-phase heat and mass transfer process in land surface models (LSMs). The potential-based equations of coupled mass and heat transport under constant air pressure form the basis of the proposed model. The model is developed considering dry air as a single phase, and including mechanical dispersion in the water vapor and dry air transfer. The adsorbed liquid flux due to thermal gradient is also taken into account. The set of equations for the two-phase heat and mass transfer is formulated fully considering diffusion, advection, and dispersion. The advantage of the proposed model over the traditional equation system is discussed. The accuracy of the proposed model is assessed through comparison with analytical work for coupled mass and heat transfer and experimental work for isothermal two-phase flow (moisture/air transfer). The influence adding airflow has on the coupled moisture and heat transfer is further investigated, clearly identifying the importance of including airflow in the coupled mass and heat transfer. How the isothermal two-phase flow is affected by considering heat flow is also evaluated, showing the influence of heat flow only to be significant if the air phase plays a significant role in solving the equations of the water phase. On the basis of a field experiment, the proposed model is compared with the measured soil moisture, temperature, and evaporation rate, the results showing clearly that it is necessary to consider the airflow mechanism in soil-atmosphere interaction studies.

Citation: Zeng, Y., Z. Su, L. Wan, and J. Wen (2011), Numerical analysis of air-water-heat flow in unsaturated soil: Is it necessary to consider airflow in land surface models?, *J. Geophys. Res.*, *116*, D20107, doi:10.1029/2011JD015835.

1. Introduction

1.1. Motivation

[2] Recent efforts to determine an optimal soil moisture (or wetness) product for the initialization of the land surface component of global weather and climate forecast models have found that the transferability of soil moisture from one land surface model to another is not straightforward [*Dirmeyer et al.*, 2004; *Koster et al.*, 2009; *Rosero et al.*, 2010]. This nontransferability is exemplified in that even when land surface models (LSMs) are driven by identical atmospheric forcing data, large differences exist between the soil moisture products generated by the different LSMs [*Dirmeyer et al.*, 2006]. This large diversity in LSMs has been an acknowledged problem since 1992, when the World Climate Research Programme (WCRP) launched the Project for the Intercomparison of Land-surface Parameterization Schemes (PILPS) [*Henderson-Sellers et al.*, 1993].

[3] To understand the large diversity, PILPS Phase 1 and 2 investigated the physical self-consistency of LSMs. The results showed that model-generated soil moisture is sensitive to the choice of soil hydraulic properties [*Shao and Henderson-Sellers*, 1996b], the initialization and the model scheme [*Pitman et al.*, 1999], and the arbitrary specification of soil depth [*Slater et al.*, 2001]. In the following PILPS Phases, a multimode land surface model (CHAmeleon Surface Model (CHASM) [*Desborough*, 1999]) was developed to investigate the impact of land-surface parameterization complexity on the simulation of land-surface climates by atmospheric models. Investigation of the impact of parameter calibration on model simulations revealed that a complex representation of land surface processes in atmospheric models is preferred to a simple one with tunable parameters, despite better performance of the latter [*Gupta et al.*, 1999]. The major reason the complex model is preferred, is attributed to its more physics-based parameterizations. *Desborough* [1999] shows that the models with more complex physics contain substantial geographic and daily functionality not present in the simpler model.

[4] Research by *Kato et al.* [2007] on the relationship between complexity and model performance highlights the

[1]School of Water Resources and Environment, China University of Geosciences, Beijing, China.
[2]Faculty of Geo-Information Science and Earth Observation, University of Twente, Enschede, Netherlands.
[3]Key Laboratory of Land Surface Process and Climate Change in Cold and Arid Region, Cold and Arid Regions Environmental and Engineering Research Institute, Chinese Academy of Sciences, Lanzhou, China.

Copyright 2011 by the American Geophysical Union.
0148-0227/11/2011JD015835

importance of calibrating LSMs and improving their physics in order to increase the accuracy of simulated soil states. Their results are identical to those stated by *Desborough* [1999]. However, it is appropriate to note that the relationship between complexity and model performance is not straightforward [*Bastidas et al.*, 2006]. Although more complex LSMs do improve simulations of soil states [*van den Hurk et al.*, 2000; *Dong et al.*, 2001; *Ek et al.*, 2003; *Miguez-Macho et al.*, 2007; *Niu et al.*, 2007; *Oleson et al.*, 2008; *Balsamo et al.*, 2009; *de Rooij*, 2010; *Zeng and Decker*, 2010], higher complexity does not always lead to increased accuracy in simulations [*Hogue et al.*, 2006; *Rosero et al.*, 2009]. Increased complexity may cause decreased model performance on an annual time scale, while being recognized as essential for realistic land surface behavior on shorter time scales [*Koster et al.*, 1999].

[5] Most LSMs used in atmospheric circulation and numerical weather prediction are simplifications of complete heat and mass transfer models in the soil, essential to reflect the impacts of the actual amount of soil moisture and energy on agriculture system, hydrology system, regional and global climate system, etc. [*Robock et al.*, 1998]. The development of LSMs addressing the coupled heat and mass transfer process in soil has been ongoing for decades [*Flerchinger and Saxton*, 1989; *Avissar and Pielke*, 1989; *Avissar*, 1992; *Braud et al.*, 1995; *Jassal et al.*, 2003], and shows promising improvement in providing good estimates of soil water content and temperature, and of surface energy balance components from bare soil. The correct calculation of the evaporation is a crucial step that subsequently affects the atmospheric modeling of boundary layer structures and cloud formations. The LSMs including the coupled process perform better than the simplified models in the evaluation of surface water vapor fluxes.

[6] Most recently, work by *Zeng et al.* [2011] includes airflow in the coupled heat and mass transfer process in soil to numerically investigate its impact on surface evaporative flux, and found that neglecting airflow can lead to an underestimation error of 33–53% on the first day after a rainfall event. The impact of the airflow induced by atmospheric pressure variation on soil-atmosphere gas exchange is a topic of discussion since *Buckingham* [1904] described the air movement in soil in response to atmospheric pressure. In terms of understanding biogeochemical cycling and global change, which form the purpose of the third-generation LSMs [*Pitman*, 2003], it is crucial to quantify any impact airflow within soil can have on the transport of CO_2 and other trace gases [*Massman*, 2006]. Nevertheless, there are few studies addressing the question whether it is feasible or necessary to consider airflow mechanisms in LSMs. This paper aims to answer that question from a subsurface physical point of view.

1.2. Subsurface Physics Background

[7] A traditional conceptual model for water flow in unsaturated soil neglects the flow-of-gas phase, as can be seen in the statement: "Unsaturated flow … is nothing but a special case of simultaneous flow of two immiscible fluids, where the nonwetting fluid is assumed to be stagnant" [*Bear*, 1972]. According to this statement, air always remains at atmospheric pressure and is free to escape from or enter into the vadose zone. This assumption is widely used in the traditional coupled moisture and heat flow model, based on the theory by *Philip and De Vries* [1957] (hereinafter PdV model, referring to this traditional model), even when water vapor movement is considered. However, the flow in porous media is actually a two-phase flow problem [*Schrefler and Zhan*, 1993], in need of complicated mathematical analysis of the response of soil to atmospheric forcing, caused by nonlinearities, moisture retention hysteresis, soil heterogeneity, as well as by multiple length and time scales [*Milly*, 1982]. The usual approach to solving the numerical model of water flow in soil involves the above cited assumption, which is often called the Richards approximation [*Celia and Binning*, 1992]. Although successful application of this assumption has been demonstrated in many cases, there are situations where the air phase can significantly retard or speed up infiltration [*Touma and Vauclin*, 1986; *Prunty and Bell*, 2007]. To properly describe these gas influenced infiltrations, a two-phase model must be used.

[8] To improve the model representation of multiphase systems, there have been continuous efforts to build comprehensive multiphase models. At present, the modern two-phase heat and mass flow models have generally overcome most of the above mentioned difficulties [*Olivella et al.*, 1996; *Pruess*, 2004], and the weaknesses of the single-phase approach have been systematically discussed in these studies. Some of the existing comprehensive multiphase models, e.g., CODE_BRIGHT [*Olivella et al.*, 1996] and TOUGH2 [*Pruess*, 2004], have been mainly applied to geothermal problems [*Zhang et al.*, 2004], without paying attention to the soil-atmosphere interacting mechanisms mentioned in section 1.1. Such comprehensive multiphase models (e.g., fluid flow in the deformable porous media) do not make including a two-phase heat and mass flow model into the land surface model straightforward. It is also not easy to understand why a two-phase flow mechanism is better than the traditional PdV model in the context of soil-atmosphere interaction. The PdV model has been widely used in many unsaturated flow simulators [*Fayer*, 2000; *Flerchinger*, 2000; *Saito et al.*, 2006; *Šimůnek and van Genuchten*, 2008], and subsequently adopted as submodel in hydrological integration models [*Twarakavi et al.*, 2008; *van Dam et al.*, 2008] and land surface models [*Avissar and Pielke*, 1989; *Avissar*, 1992; *Braud et al.*, 1995; *Jassal et al.*, 2003]. Therefore, in aiming to understand the need to include a two-phase flow mechanism in LSMs, it is necessary to know how the airflow influences the performance of the PdV model when simulating soil moisture and soil temperature.

[9] On the other hand, the isothermal two-phase fluid flow in unsaturated soil, excluding heat flow and transport (e.g., considering air-water flow only), has seen an increase in development because of its indispensable role in simulating, modeling and studying waste storage, geological storage, underground natural resource recovery and environmental remediation, etc. [*Wu and Forsyth*, 2001, *Celia and Nordbotten*, 2009]. However, most development has been focusing on multiscale problems or numerical formulations and solutions [*Celia et al.*, 1993; *Ataie-Ashtiani and Raeesi-Ardekani*, 2010], and very little attention has been paid to investigating how heat flow can affect the isothermal two-phase flow (air-water flow only) in the soil.

1.3. Focus of Paper

[10] In order to illuminate, from a physical point of view, the influence of airflow on the PdV model and the effect of heat flow on an isothermal two-phase flow model (air-water flow only), a two-phase heat and mass flow model (one-dimensional) is developed. This model considers diffusion, advection and dispersion mechanisms. The matric head-based equations of *Milly* [1982] are adopted as the basis for a mass balance equation of soil moisture. In addition to the existing mechanisms included in Milly's model, the effects of the thermal liquid flux and of the dry air phase (i.e., dispersive water vapor flux, and water vapor flux as part of the bulk flow of dry air) are considered. The mass balance equation for dry air includes both the bulk flow of dry air and the air dissolved in liquid. All conduction, advection, dispersion, latent heat of vaporization, and differential heat of wetting are represented in the energy balance equation. The latter is the amount of heat released when a small amount of free water is added to the soil matrix [*deVries*, 1958]. On the basis of the conservation equations of moisture, dry air, and energy, three coupled partial differential equations are solved simultaneously using the Galerkin residual finite element method.

[11] This paper is structured along the following lines. In section 2, development of the new model is discussed, taking water vapor diffusion, advection and dispersion mechanisms into account, based on the traditional coupled moisture and heat flow model (PdV model). In section 3, published numerical and experimental studies are used to verify the developed model. Verification of the new model is performed in two steps. First, the capacity to describe the two-phase flow under isothermal conditions (air-water flow only) is investigated, based on infiltration experiments by *Touma and Vauclin* [1986, hereinafter TV86]. Second, the capacity to simulate coupled heat and mass flow under constant air pressure (PdV model) is examined, comparing the simulation results with the analytical results presented by *Milly* [1982]. Furthermore, a numerical modeling study is carried out to illuminate the significance of including the air-phase flow in the PdV model, and of including the heat flow in the isothermal two-phase flow (air-water flow only) model. In the final part of section 3, a field application is presented based on the verified model. Conclusions are drawn in section 4.

2. Governing Equations

[12] Two main groups of equations, i.e., conservation equations and related parameterizations (see Appendix A), are used to describe the two-phase heat and mass flow model. The Milly's equations, predominantly considering the vertical interactive process between atmosphere and soil, are introduced first to describe the traditional coupled moisture and heat flow model scheme (PdV model). On the basis of that, the two-phase heat and flow model is developed. Considering dry air as a single phase and the main component of the gaseous phase in soil, the balance equation for dry air is introduced subsequently. Henry's law is used to express the equilibrium for dissolved air in liquid. In addition, the thermal equilibrium assumption between the phases is adopted and the equation for energy balance evaluated, taking into account the internal energy in each phase (liquid, water vapor, and dry air).

2.1. Balance Equations

2.1.1. Soil Water Conservation Equation

[13] The water in soil is present in a liquid and in a gaseous phase, and following *Milly* [1982], the total moisture balance is expressed as

$$\frac{\partial}{\partial t}(\rho_L\theta + \rho_V\theta_a) = -\frac{\partial}{\partial z}q_m \tag{1}$$

where ρ_L(kg m^{-3}) represents the density of liquid water; θ(m^3 m^{-3}) the volumetric water content; θ_a(m^3 m^{-3}) the gas phase volumetric content; z(m) the vertical space coordinate, positive upwards; and q_m(kg m^{-2} s^{-1}) the soil moisture flux in both the liquid and the vapor phase. The latter can be tentatively expressed as [*Milly*, 1982]

$$q_m = q_L + q_V = -\underbrace{\rho_L K\frac{\partial(h+z)}{\partial z}}_{\substack{liquid\\ Convection}} - \underbrace{\rho_L D_{TD}\frac{\partial T}{\partial z}}_{\substack{Thermal\\ liquid\\ Convection}} - \underbrace{D_e\frac{\partial \rho_V}{\partial z}}_{\substack{Vapor\\ Diffusion}} \tag{2}$$

where q_L(kg m^{-2} s^{-1}) is the liquid flux; q_V(kg m^{-2} s^{-1}) the water vapor flux; K(m s^{-1}) the hydraulic conductivity; h(m) the matric potential; D_{TD}(m^2 s^{-1} °C^{-1}) the transport coefficient for adsorbed liquid flow due to the temperature gradient; D_e(m^2 s^{-1}) the molecular diffusivity of water vapor in soil; ρ_V(kg m^{-3}) the density of water vapor; and T(°C) the soil temperature.

[14] In the right hand side (RHS) of equation (2), the first two terms represent the liquid flux and can be divided into three components, respectively; the first component depending on the moisture gradient, the second depending on the gravity and the third on the temperature gradient. The last term in equation (2) represents the water vapor flux, which can be separated into an isothermal and a thermal component, considering that the density of water vapor is a function of matric potential and temperature.

[15] If the following assumptions are made: (1) dry air is considered to be a single phase, and (2) the water vapor flow is assumed to be induced in three ways: first by diffusive transfer, driven by the water vapor pressure gradient; second by advective transfer, as part of the bulk flow of air; and third by dispersive transfer, due to the longitudinal dispersivity of water vapor, which is a function of water vapor saturation; then equation (2) may be rewritten as [*Thomas and Sansom*, 1995]

$$q_m = -\rho_L\left[\underbrace{K_{Lh}\frac{\partial}{\partial z}\left(h+\frac{P_g}{\gamma_w}\right)}_{\substack{Liquid\\ Convection}} + \underbrace{(K_{LT}+D_{TD})\frac{\partial T}{\partial z}}_{\substack{Thermal\\ Liquid\\ Convection}} + K_{Lh}\right] - \left[\underbrace{D_e\frac{\partial \rho_V}{\partial z}}_{\substack{Vapor\\ Diffusion}} - \underbrace{\rho_V\frac{q_a^a}{\rho_{da}}}_{\substack{Vapor\\ Convection}} + \underbrace{(\theta_a D_{Vg})\frac{\partial \rho_V}{\partial z}}_{\substack{Vapor\\ Dispersion}}\right] \tag{3}$$

in which K_{Lh}(m s^{-1}) is the isothermal hydraulic conductivity; K_{LT}(m^2 s^{-1} °C^{-1}) the thermal hydraulic conductivity ($K = K_{Lh} + K_{LT}$); Pg (Pa) the pore-air pressure; γ_w(kg m^{-2} s^{-2}) the specific weight of water ; q_a^a(kg m^{-2} s^{-1}) the advective dry air flux (discussed in equation (5)); ρ_{da}(kg m^{-3}) the density of dry air; and D_{Vg}(m^2 s^{-1}) the gas phase longitudinal dispersion coefficient.

[16] The terms within the first set of square brackets in equation (3) represent the liquid flux. The term (P_g/γ_w) is the atmospheric pressure expressed as the height of a water column. The terms within the second set of square brackets represent the water vapor flux, with the first term (already present in equation (2)) representing the diffusive flux (Fick's law), the second representing the advective flux (Darcy's law) and the third the dispersive flux (Fick's law).

[17] Equation (2) shows clearly that only thermal and isothermal liquid advection and water vapor diffusion are considered in the traditional coupled heat and mass transport model (PdV model). However, equation (3) shows that dry air is considered a single phase. Thus not only diffusion, but also advection and dispersion become included in the water vapor transport mechanism. As for the liquid transport, the mechanism remains the same, but with atmospheric pressure acting as the driving force gradient.

2.1.2. Dry Air Conservation Equation

[18] Dry air transport in unsaturated soil is driven by two main gradients: the dry air concentration or density gradient and the mixed soil air pressure gradient. The first one diffuses the dry air in soil pores, while the second one causes an advective flux of dry air. At the same time, the dispersive transfer of dry air should also be considered. In addition, considering the mechanical and chemical equilibrium, a certain amount of dry air will dissolve into liquid according to Henry's law. Considering the above four effects, the dry air mass conservation may be written as [*Thomas and Sansom*, 1995]

$$\frac{\partial}{\partial t}[\varepsilon \cdot \rho_{da}(S_a + H_c S_r)] = -\frac{\partial}{\partial z} q_a \tag{4}$$

with

$$q_a = -D_e \frac{\partial \rho_{da}}{\partial z} - \rho_{da} \frac{S_a k_g}{\mu_a} \frac{\partial P_g}{\partial z} + H_c \rho_{da} \frac{q_L}{\rho_L} - \left(\theta_a D_{Vg}\right) \frac{\partial \rho_{da}}{\partial z} \tag{5}$$

where ε is the porosity; q_a(kg m^{-2} s^{-1}) the dry air flux; k_g(m^2) the intrinsic air permeability; μ_a(= 1.846 × 10^{-5} kg m^{-1} s^{-1}) the air viscosity; S_a(= 1 − S_r) the degree of air saturation in the soil; S_r (= θ/ε) the degree of saturation of the soil; H_c(= 0.02) Henry's constant. In the RHS of equation (5), the first term depicts the diffusive flux (Fick's law), the second term the advective flux (Darcy's law, $q_a^a = -\rho_{da} \frac{S_a k_g}{\mu_a} \frac{\partial P_g}{\partial z}$), the third term the advective flux due to dissolved air (Henry's law), and the fourth the dispersive flux (Fick's law).

2.1.3. Energy Balance

[19] In the vadose zone, the mechanisms for energy transport include conduction and advection. The conductive heat transfer contains the contribution from liquids, solids and gas. Conduction is the main mechanism for heat transfer in soil and contributes to the energy conservation in solids, liquids and air. Advective heat in soil is conveyed by liquid flux, water vapor flux, and dry air flux. On the other hand, the heat storage in soil includes the bulk volumetric heat content, the latent heat of vaporization and a source term associated with the exothermic process of wetting of a porous medium (integral heat of wetting) [*deVries*, 1958]. Following the general approach of *deVries* [1958], the energy balance equation in unsaturated soil may be written as

$$\begin{aligned}\frac{\partial}{\partial t}[(\rho_s\theta_s c_s + \rho_L\theta c_L + \rho_{da}\theta_a c_a + \rho_V\theta_a c_V)(T - T_r) + \rho_V L_0\theta_a] - \rho_L W\frac{\partial\theta}{\partial t} \\ = \frac{\partial}{\partial z}\left(\lambda_{eff}\frac{\partial T}{\partial z}\right) - \frac{\partial}{\partial z}[q_L c_L \cdot (T - T_r) + q_V(L_0 + c_V \cdot (T - T_r)) \\ + q_a c_a \cdot (T - T_r)]\end{aligned} \tag{6}$$

where c_s, c_L, c_a and c_v(J kg^{-1} °C^{-1}) represent the specific heat of solids, liquids, dry air and water vapor, respectively; ρ_s(kg m^{-3}) the density of solids in the soil; θ_s the volumetric content of solids in the soil; T_r(°C) the arbitrary reference temperature; L_0(J kg^{-1}) the latent heat of vaporization of water at temperature T_r; W(J kg^{-1}) the differential heat of wetting (the amount of heat released when a small amount of free water is added to the soil matrix); and λ_{eff}(W m^{-1} °C^{-1}) the effective thermal conductivity. If the advective flux conveyed by the dry air flux ($q_a c_a \cdot (T - T_r)$) and the bulk volumetric heat content of dry air ($\rho_{da}\theta_a c_a$) were neglected, equation (6) would result in the heat balance equation of *Milly* [1982].

2.2. Numerical Approach

[20] The governing differential equations are converted to nonlinear ordinary differential equations with unknowns as the independent variables (soil matric potential, soil temperature and soil air pressure) at a finite number of nodes in Galerkin's method of weighted residuals. A finite difference time stepping scheme is then applied to evaluate the time derivatives, and is solved by a successive iterative linearization scheme. The governing equations subject to the boundary and initial conditions are solved numerically by an author-developed script with MATLAB (The Math-Works Inc., Natick, Massachusetts, Version 7.8.0.347(R2009a)). To achieve the desired convergence criteria, following *Milly and Eagleson* [1980], the prescribed upper limits of moisture content, matric potential, temperature and pressure are used to determine a new time step size automatically in the form of

$$\Delta t = \min\left[\frac{X_{\max}}{\max_i\left(\frac{d\theta_i}{dt}\right)}, \frac{T_{\max}}{\max_i\left(\frac{dT_i}{dt}\right)}, \frac{P_{g_{\max}}}{\max_i\left(\frac{dP_{g_i}}{dt}\right)}, \frac{h_{\max}}{\max_i\left(\frac{dh_i}{dt}\right)}\right] \tag{7}$$

where $\max_i$ denotes maximization over all nodes i, and the changes in state variables are estimated from the most recent time step; $X_{\max}$ is the upper limit of change for volumetric water content; $T_{\max}$ for temperature; $P_{g\max}$ for atmospheric pressure; and $h_{\max}$ for matric potential. If the change exceeds

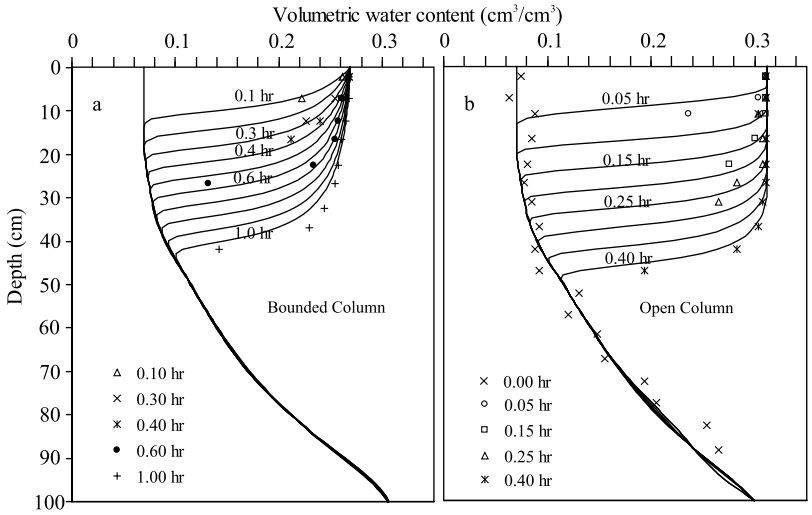

Figure 1. Comparison of the simulated water profiles (solid lines) in the (a) bounded and (b) open soil columns based on the data obtained in the TV86 experiment (data points) (adapted from Figure 5 of TV86).

the desired upper limit, the calculation of that time step is erroneous, and the time step is repeated with a decreased time length. By doing this, a reasonable tradeoff between computational effort and accuracy of the solution should be achieved.

3. Numerical Results and Discussions

3.1. Model Verification

[21] Model performance was assessed against two benchmark studies. First, to verify the algorithm and to examine details of the isothermal two-phase flow, the experiments and associated numerical simulations of TV86 were used. Second, to verify the simultaneous transport of moisture and heat under constant atmospheric pressure, a strong coupling problem solved analytically and numerically by *Milly* [1982] was employed.

3.1.1. Case of TV86

[22] The first verification of the model to be undertaken was to compare its outputs with published experiment data and numerical solutions for a two-phase air-water system. Several one-dimensional transient problems, including both flux and ponded experiments, are reported in TV86. The ponded experiment was performed by imposing a time constant positive water head (2.3 cm) at the surface using a Mariotte bottle device. The flux experiment was designed to apply time constant water fluxes (8.3 cm h^{-1} and 20 cm h^{-1}) at the surface, supplied by means of a volumetric pump through a series of 20 hypodermic needles. In this section, only the ponded experiment was used to verify the proposed model.

[23] In accordance with TV86, the soil air and water hydrodynamic characteristics were determined by laboratory measurement. The water retention curve was fitted using the Van Genuchten model with the following parameters: θ_{res} = 0.0265, θ_{sat} = 0.312, α = 0.044 cm^{-1} and n = 2.2. TV86 stated that the natural water saturation (θ_{sat}) was significantly smaller than the porosity (ε = 0.37) because of air entrapment and that the residual water content (θ_{res}) had to be viewed only as a fitting parameter and not necessarily as the actual residual water content. The air entry pressure was estimated at h_{ae} = 14 cm of water. The hydraulic conductivity functions used were

$$K_{Lh} = A_w \theta^{B_w} \tag{8}$$

where, as in TV86, the two parameters are A_w = 18130 cm h^{-1} and B_w = 6.07, implicitly entailing that $K_{Lh} = K_s$ = 15.4 cm h^{-1} when $\theta = \theta_{sat}$, and,

$$K_a = K_{as} \frac{A_a}{A_a + h^{B_a}} \tag{9}$$

where, as in TV86, the three parameters are $A_a = 3.86 \times 10^{-5}$, B_a = −2.4 and K_{as} = 2800 cm h^{-1}.

[24] In order to check the influence of airflow on the infiltration, numerical experiments were conducted with bounded bottom and open bottom. In the open bottom case, the air was able to escape freely and infiltration was in accordance with the Richards water flow approximation (single-phase flow). However, when the column was bounded, the infiltration process was significantly retarded. The soil column, with a length of 100 cm, was vertically discretized into 100 elements, which is equivalent to 101 nodes with Δz = 1 cm. Variable time stepping was applied with an initial time step of Δt = 1 s. The initial soil water content was obtained from TV86 [TV86, Figure 5], and is symbolized by a cross sign (×) in Figure 1b. The initial condition was obtained by draining the saturated soil column to the static equilibrium corresponding to a piezometric level at 120 cm below the surface. In accordance with to the experimental setup by TV86, the boundary conditions were described as:

$$\begin{aligned}
&h(z,t) = 2.3 \text{ cm} && t > 0 && z = 0 \text{ cm} \\
&q_a(z,t) = 0 && 0 \le t < t_{crit} && z = 0 \text{ cm} \\
&P_g(z,t) = h_{ae} + 2.3 && t \ge t_{crit} && z = 0 \text{ cm} \\
&q_L(z,t) = 0 && t \ge 0 && z = L = -100 \text{ cm} \\
&q_a(z,t) = 0 && t \ge 0 && z = L = -100 \text{ cm}
\end{aligned} \tag{10}$$

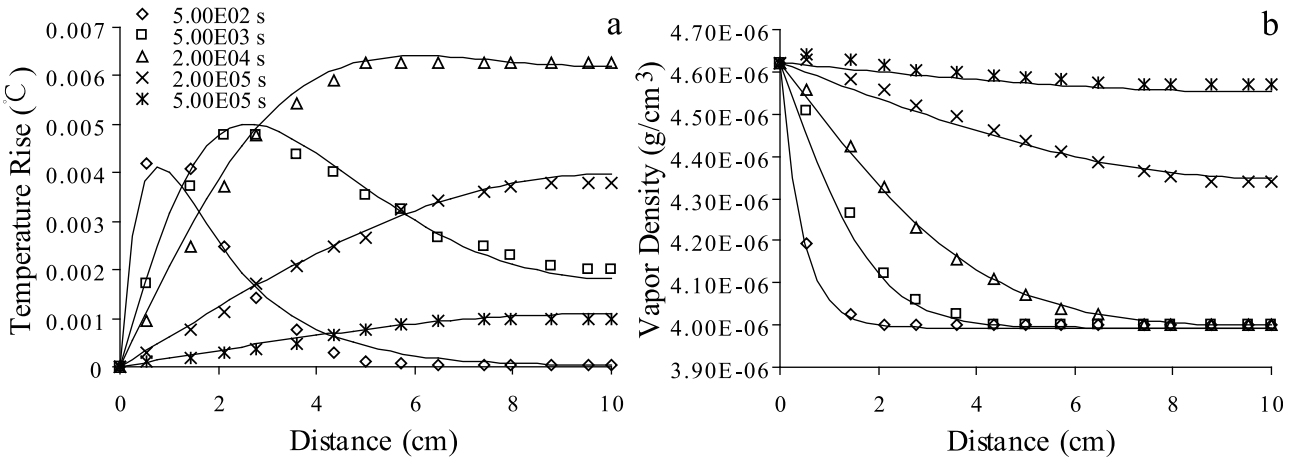

Figure 2. Comparison between the simulated (solid lines) soil (a) temperature rise and (b) water vapor density based on the data obtained in Milly's experiment (data points) (adapted from Figure 8 of *Milly* [1982]).

$$\begin{aligned} h(z,t) &= 2.3 \text{ cm} \quad t > 0 \quad z = 0 \text{ cm} \\ h(z,t) &= -5.8 \text{ cm} \quad t \geq 0 \quad z = -100 \text{ cm} \end{aligned} \tag{11}$$

Equation (10) depicts the boundary conditions used in the modeling of the experiment run in the bounded column, and equation (11) depicts the open column case. In the bounded column experiment, the time t_{crit} denoted the moment at which the pressure on the surface reached the value of h_{ae} +2.3 cm, above which the air freely escaped from the surface through the ponded water. In TV86's case, t_{crit} was determined to be at 12 s. Notice that the depth of ponding on the surface is 2.3 cm. In the open column experiment, the boundary conditions were simpler than in the bounded column experiment, because the air could freely escape from the bottom of the column. This free escape of the air prevented an increase of air pressure in the column, and as a result no air escaped from the surface through the ponded water.

[25] Figure 1 shows satisfactory agreement between the data points and the simulation results. As can be seen in Figures 1a and 1b, the infiltration obviously occurred faster in the open column than in the bounded column. After 0.4 h of infiltration, the wetting front reached a depth of about 50 cm in the open column, while reaching a depth of about 25 cm in the bounded column. The three major differences between the water content profiles in the open column and the bounded column are in excellent agreement with TV86's findings: first, the infiltration rate is drastically reduced when air cannot escape from the bounded bottom; second, the slopes are less abrupt when air phase transport is considered; third, because of the escape of air from the top of the column, the saturation water content is around 0.27, compared to 0.312 when only the liquid phase transport is considered. These results demonstrate the ability of the proposed model to analyze the two-phase flow.

3.1.2. Case of *Milly* [1982]

[26] The second verification of the model to be undertaken was a comparison with Milly's solution for simultaneous mass and heat transport in a very dry soil. The basic idea is that water vapor diffusion in a vapor-dominated system (very dry soil) will cause water vapor condensation and consequently the release of latent heat, thus causing a temporary rise in the medium temperature. Subsequently, as the heat flux diffuses out of the system, the medium temperature will return to its original value. In order to check this, a sudden increase in water vapor supply was applied at one end of the soil column to examine the strong coupling process between moisture and heat fields.

[27] Yolo light clay soil was used in this case, for which the water retention curve written by *Haverkamp et al.* [1977] was

$$\theta = \begin{cases} 0.371 \cdot \left[1 + \left(\dfrac{\log(|h|)}{2.26}\right)^4\right]^{-1} + 0.124, & h < -1 \text{ cm} \\ 0.495, & h \geq -1 \text{ cm} \end{cases} \tag{12}$$

The hydraulic conductivity was given as [*Haverkamp et al.*, 1977]

$$K_{Lh} = K_s \cdot \left[1 + \left(\frac{|h|}{15.3}\right)^{1.77}\right]^{-1}, K_s = 1.23 \times 10^{-5} \text{ cm/s} \tag{13}$$

The volumetric heat capacity was expressed as the first term in the square bracket of the left hand side (LHS) of equation (6) without considering dry air, in which $c_s = 0.47$, $c_L = 4.18$, and $c_v = 1$ (10^{-3} J kg^{-1} °C^{-1}). The soil specimen, with a length of 10 cm, was discretized vertically into 40 elements of 0.25 cm length. A convenient constant time stepping of 500 *s* was used for comparison with Milly's results. The boundary and initial conditions selected were expressed as:

$$\begin{aligned} &\rho_v(z,t) = \overline{\rho} && t = 0 \quad -10 \text{ cm} \leq z \leq 0 \text{ cm} \\ &T(z,t) = \overline{T} && t = 0 \quad -10 \text{ cm} \leq z \leq 0 \text{ cm} \\ &\rho_v(z,t) = \overline{\rho} + \Delta\rho && t > 0 \quad z = 0 \text{ cm} \\ &T(z,t) = \overline{T} && t > 0 \quad z = 0 \text{ cm} \\ &\partial\rho_v/\partial z = 0 && t > 0 \quad z = -10 \text{ cm} \\ &\partial T/\partial z = 0 && t > 0 \quad z = -10 \text{ cm} \end{aligned} \tag{14}$$

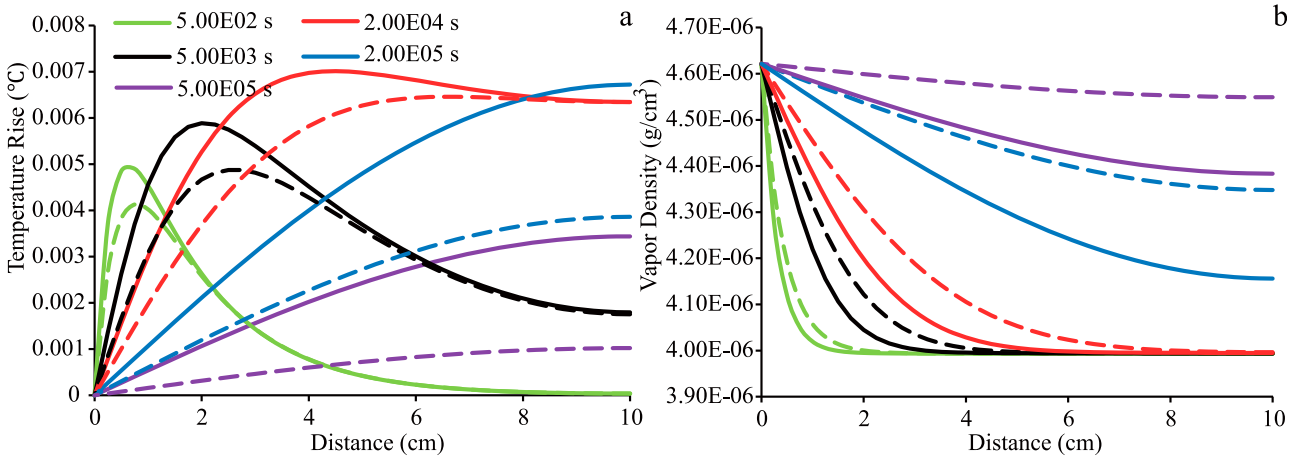

Figure 3. Comparison of (a) temperature rise and (b) water vapor density profiles, with (solid line) and without (dashed line) considering the air balance equation.

The following numerical values were selected for the solution:

$$\overline{\rho} = 4.03 \times 10^{-6}\text{g cm}^{-3}, \Delta\rho = 0.63 \times 10^{-6}\text{g cm}^{-3}, \overline{T} = 20°\text{C} \quad (15)$$

Figure 2 shows excellent agreement between the simulation results (solid lines) and Milly's results. Figure 2a shows that the sudden increase of water vapor supply on the surface raised the temperature near the surface steeply. As time elapsed, the temperature slowly reassumed its original value, as the soil specimen was equilibrated to the water vapor supply on the surface. In Figure 2b, the propagation of water vapor density depicts the water vapor balancing process during water vapor diffusion into soil. As time elapsed, the difference in water vapor density between the top and the bottom of the specimen approached zero. After long enough diffusion, the whole soil specimen would have a constant temperature and water vapor density. The success of this test case established the validity of the proposed model for modeling simultaneous heat and mass transfer in soil.

3.2. Numerical Analysis

3.2.1. Influence of Airflow in Milly's Case

[28] In Milly's case, the gas phase flow in the unsaturated zone is considered in order to include only water vapor flux, while the dry air is assumed to be an inert gas. This assumption avoids the calculation of the complete air balance equation, though air may have a significant influence on the water vapor flux. As known from TV86's case, infiltration is retarded in the bounded column because of the effect of the air pressure in the soil. In this study, a 10 cm thick specimen was bounded to test the air effect on the coupled moisture and heat transport.

[29] The simulation result shows that the transport of water vapor in soil displayed a similarly retarded phenomenon, caused by the outward air pressure gradient, which in turn was induced by the temperature rise due to the water vapor condensation. As can be seen in Figure 3b, water vapor penetration was slowed down. Given the same time elapsed, the water vapor density profiles considering airflow (solid lines) is obviously farther away from reaching the equilibrium, than those (dashed lines) that did not consider the air balance equation. At the same time (Figure 3a) the absolute temperature rise increased (the solid lines are above the dashed lines) because of retardation in the water vapor transport, causing more water vapor to be condensed and more heat to be released.

[30] A note of caution about Figures 2 and 3, however, is appropriate here. The scale of both temperature rise (10^{-3} °C) and vapor density (10^{-6} g cm^{-3}) was quite small and hardly detectable using instrumentation. However, the small scale is intended that the analytical solution for the Milly's case (e.g., strong coupling between moisture and heat fields), is feasible. The analytic solution for Milly's case required a small perturbation of the system and simplified assumptions [*Milly*, 1982] (i.e., the simultaneous transport of soil moisture and heat is carried only by vapor diffusion, and the sensible heat carried by water vapor is negligible). In order to match the requirements for the analytic solution, the numerical experiment was set up along equations (14) and (15). According to equation (15), the percentage of perturbation of the water vapor supply was less than 16%, causing the medium temperature to vary from 20°C to 20.0065°C (0.032% variation) (Figure 2). The capture of this undetectable variation (analytic solutions) by the model demonstrated its capability to simulate the dynamics of vapor-dominated systems with strong coupling between moisture and heat fields.

[31] The aim of section 3.2.1 was to check how airflow affected the coupled dynamics. Figure 3 shows that the inclusion of airflow, using the proposed model from section 2, decreased the vapor density and increased the temperature rise. The air effect should be quantified as absolute and as relative effect. The absolute air effect was calculated from absolute differences between the integrated areas under the solid (with air) and the dashed (without air) lines in Figures 3a and 3b, i.e., the area between the green solid line and the green dashed line indicates the absolute difference caused by the air effect. The relative air effect was calculated by dividing the absolute differences into the integrated areas under the dashed lines (without air) and was expressed as a percentage, i.e., the absolute difference between the green solid line and the green dashed line is

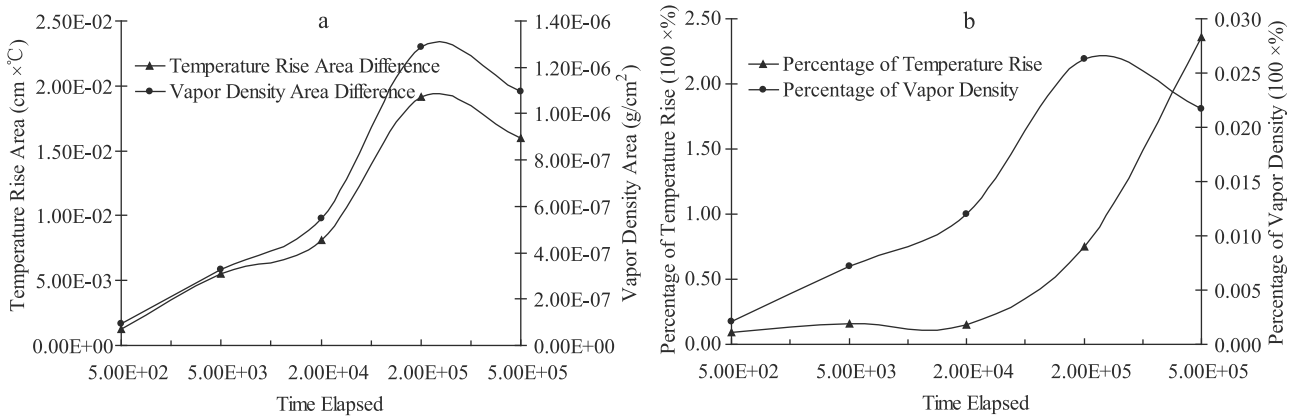

Figure 4. (a) The absolute air effect expressed as the absolute difference between the integrated areas under the solid lines (with air) and dashed lines (without air) in Figures 3a and 3b; (b) the relative air effect expressed as percentage of the absolute difference to the integrated areas under the dashed lines.

divided by the integrated area under the green dashed line. Figure 4a shows that the absolute air effect increased as time elapsed, till 2.00E05 *s*, and weakened afterwards for both temperature rise and vapor density. Compared to the undetectable absolute variation in Milly's case, the relative air effect demonstrated better how airflow affected the coupled dynamics. Figure 4b shows that the relative air effect of vapor density had the same variation as the absolute one, while the relative effect on the temperature rise showed a different pattern.

[32] Relatively, the air effect on the temperature rise increased further after 2.00E05 s, instead of being weakened (Figure 4b). This increase actually explains the effect of the retardation in the water vapor transport, which caused more water vapor to be condensed and more heat to be released. The averaged percentages of the relative air effect on the temperature rise and the vapor density were 70.1% and 1.39%, respectively. Because of the extremely small temperature rise (<0.0011°C) at the end (5.00E05 *s*) of the experiment run without airflow, the small air effect caused a huge perturbation (236%) to the temperature rise at that time point, increasing the averaged percentage of the relative air effect on the temperature rise. Without considering this final perturbation, the averaged percentage of the relative air effect on temperature rise was 28.7%.

3.2.2. Influence of Heat Flow in TV86's Case

[33] For TV86's case, the ponding infiltration was examined in section 3.1.1. Their work contains two more experiments: (1) a constant water flux of 8.3 cm h^{-1}, smaller than the saturated hydraulic conductivity applied at the surface, and (2) a constant water flux of 20 cm h^{-1}, greater than the saturated hydraulic conductivity applied at the surface. These two experiments were numerically replicated, both with and without considering the heat flow and transport. Not only were water fluxes different from the saturated hydraulic conductivity (15.4 cm h^{-1}) adopted as surface boundary condition, but the open and closed bottoms discussed in section 3.2.1 were also included as boundary conditions. The lower boundary conditions for these two problems were the same as those described in equations (10) and (11). In order to investigate how the heat flow influenced the two-phase flow process, two infiltration experiments were set up: one experiment was designed to have a uniform temperature profile of 20°C during the whole simulation period (this experiment was named isothermal infiltration); the other one was set up providing a 10°C increase in temperature at the surface (30°C), while the bottom was kept at its original value (20°C) during the whole simulation period (this experiment was named thermal infiltration).

[34] Figure 5 does not show a large difference in the propagation of water content profiles in the isothermal and thermal infiltration. However, the wetting front did move slightly faster in the thermal infiltration than in the isothermal infiltration for both the open (Figure 5b) and the bounded column (Figure 5a). The movement of the wetting front was judged by the slope of the water content profiles. Figure 5a shows the slope of the water content profiles to be more abrupt in the thermal infiltration (slope = 3.38) than in the isothermal infiltration (slope = 1.7). In Figure 5b, the slope of the moisture profile in the thermal infiltration (slope = 5.5) is also steeper than in the isothermal infiltration (slope = 3.3). This indicates that a certain amount of water, supposed to be stored at certain depth in the isothermal infiltration, was partially pushed down by the thermal liquid flux in the thermal infiltration. Therefore, at the same instant, the thermal infiltration caused the soil to be less wet than the isothermal infiltrated soil at a certain depth. The volume of the water pushed down to the wetting front, was calculated by integrating the highlighted gray areas between the water content profiles in the isothermal infiltration and the thermal infiltration.

[35] Apart from the temperature effect, the two-phase isothermal infiltration with a prescribed flux rate of 8.3 (cm h^{-1}) at the top boundary, showed no big difference between the open column and the bounded column in the propagation of soil moisture (Figures 5a and 5b). Unlike in the first case in section 3.1.1, there was no ponded water at the surface, because of the fact that the flux was lower than the saturated hydraulic conductivity, which meant that the infiltration rate was limited to 8.3 cm h^{-1}. Nevertheless, the surface soil wetness was slightly greater in the bounded column than in the open column, and thus the slope of the moisture profile in the bounded column (slope = 1.7) was less steep than in the open column (slope = 3.3). As *Celia and Binning* [1992]

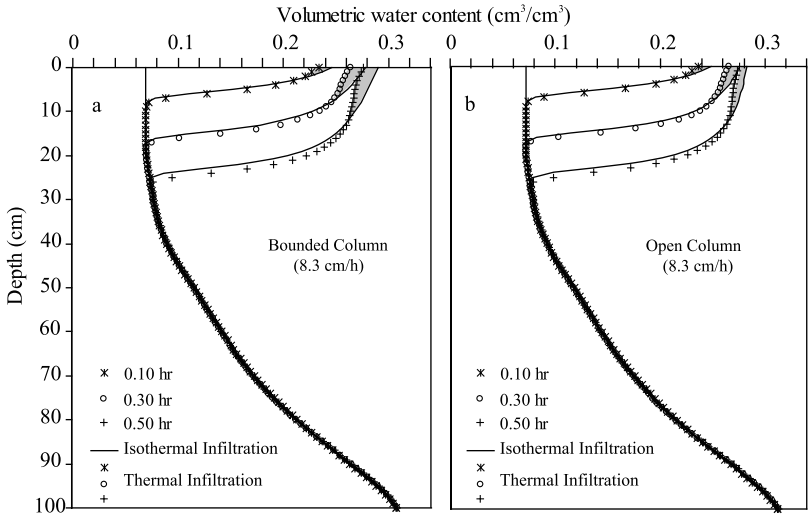

Figure 5. Time evolution of the water content profile under an infiltration rate of 8.3 (cm h^{-1}), with and without considering the heat flow in (a) a bounded and (b) an open column.

pointed out, the air flux coming out of the top of the column would have to be essentially the same as the water going in, but flowing in the opposite direction. This opposite air flux did influence the water flux going in. As a result, a certain amount of water was held back, increasing the surface wetness. This phenomenon was in accordance with the transport of water vapor into soil discussed in Milly's case (section 3.2.1), where air phase transport was considered.

[36] Figure 6 shows the propagation of soil moisture with a prescribed flux at the surface higher than the saturated hydraulic conductivity (20 cm h^{-1}), causing ponded water to build up at the surface. With the buildup of ponded water at the surface, the infiltration in the bounded column showed very clear retardation compared to the infiltration in the open column. This was in accordance with the first case discussed in section 3.1.1. However, considering the temperature effect in the isothermal two-phase flow, the differences between the moisture profiles in the isothermal and the thermal infiltration were more obvious in the bounded column (Figure 6a) than in the open column (Figure 6b). This is also evident in Figure 5, which shows the differences in moisture profiles were more obvious in the bounded column (Figure 5a) than in the open column (Figure 5b) (i.e., the highlighted gray areas in Figure 5a are larger than those in Figure 5b).

[37] The open column actually provided a path for the air to escape, creating a condition for the air in the soil column to equilibrate quickly with the atmospheric pressure, which meant that the air phase essentially had an infinitesimal effect on the solution of the equations for the water phase. However, when the column was sealed (no air escape from the bottom) and the top of the column saturated or close to saturation (no air escape from the top until the air entry value is reached), the air phase transport became a significant factor during the transient infiltration, as the results show in Figures 1 and 6. In the case of surface boundary

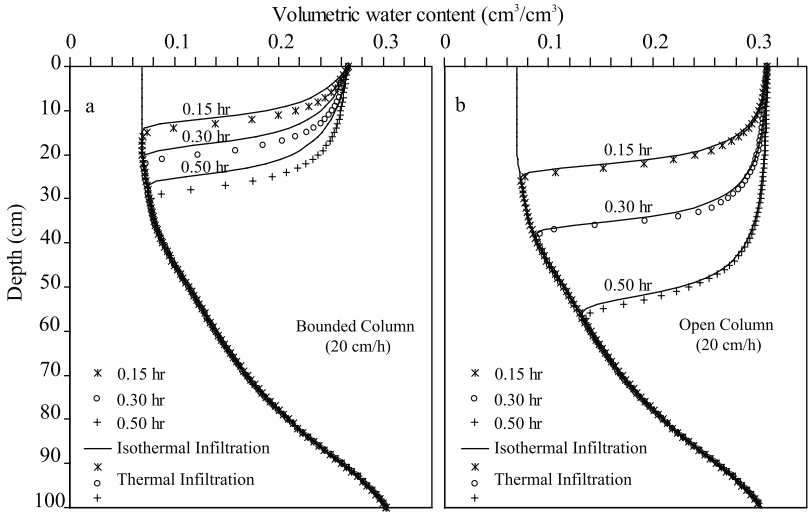

Figure 6. Time evolution of the water content profile under an infiltration rate of 20 (cm h^{-1}), with and without considering the temperature effect in (a) a bounded and (b) an open column.

flux with a hydraulic conductivity lower than its saturated value, the top of the column was not saturated and air escaped freely from the top, but nevertheless the air phase slightly affected the water phase transport (Figure 5). When the air phase effect plays a significant role in solving equations of the water phase, the inclusion of the heat flow becomes necessary. This necessity is clearly evident in Figure 6.

3.3. Field Application

[38] The field experiment was conducted at one flat dune foot in the Badain Jaran Desert (between 39°45′20″ *N* to 39°47′27″ *N* and 102°27′07″ *E* to 102°28′58″ *E*), in the northwest of the Alashan plateau in the western Inner Mongolia of China. The details on the field site and the observations made have been introduced by *Zeng et al.* [2009]. To apply the proposed model in the field, boundary conditions and forcing field had to be defined.

3.3.1. Boundary Conditions

[39] For this specific case, no ponding or surface runoff was considered. This means that the moisture flux out of the soil is always equal to evaporation minus precipitation.

$$q_m|_{z=0} = E - \rho_L P \tag{16}$$

where E(kg m^{-2} s^{-1}) is the evaporation rate; P(m s^{-1}) the precipitation rate. Considering the aerodynamic resistance and soil surface resistance to water vapor transfer from soil to atmosphere, the evaporation is expressed as [*Camillo and Gurney*, 1986]

$$E = \frac{\rho_{vs} - \rho_{va}}{r_a + r_s} \tag{17}$$

where ρ_{vs}(kg m^{-3}) is the water vapor density at the soil surface; ρ_{va}(kg m^{-3}) the atmospheric vapor density; r_s(s m^{-1}) the soil surface resistance to water vapor flow; and r_a(s m^{-1}) the aerodynamic resistance. Equation (16) forms the surface boundary condition for moisture transport. Without taking ponding and surface runoff into consideration, soil surface was open to the atmosphere and the measured atmospheric pressure was adopted as the surface boundary condition for dry air transport in the soil. The measured soil surface temperature was set as the boundary condition for heat transport.

[40] In the Badain Jaran Desert, according to *Gates et al.* [2008], the thickness of unsaturated zone ranges from less than 1 m in interdune areas to approximately 400 m in large dunes. In this study, the length of the soil column was set to be 5 m. The bottom boundary condition for the moisture equation was free drainage (unit hydraulic head gradient). Considering the diurnal variation scale, the temperature gradient and the air pressure gradient at the bottom of the column were specified to be zero. A one-dimensional setting was adopted in this study, predominantly considering the vertical interactive process between the atmosphere and the soil [*Milly and Eagleson*, 1980]. The initial soil matric head and soil temperature were determined by interpolating the measured values at midnight on 12 June 2008 between measurement depths. The initial soil air pressure was set according to the daily average atmospheric pressure during the selected 6 d period.

3.3.2. Meteorological Forcing Data

[41] In terms of finding a balance between computational efficiency and solution accuracy, the time step was required to be small enough for the moisture content and temperature not to exceed prescribed limits [*Milly and Eagleson*, 1980]. This meant that the time step was adjusted automatically during computing (1 to 1800 s). Accordingly, the time interval of the meteorological inputs was adjusted to match each new time step. In this study, the Fourier transform method was used to approximate the frequency domain representation of the meteorological forcing data, and continuously produced the forcing data.

[42] Figure 7 shows the measurement and the approximation of meteorological variables, including air temperature, relative humidity, wind speed, precipitation, atmospheric pressure, and soil surface temperature (Figures 7a–7f), measured in the Badain Jaran Desert at a height of 2 m above the soil surface, and at 30 min intervals. The 6 d data were chosen to include a rainfall event at the end of the first day of the selected period. Except for wind speed data fluctuating irregularly because of inherent randomness, the records of other variables showed clearly typical diurnal behavior.

[43] Figure 7a shows that the average air temperature was 24.3°C 1 d before the rainfall and 20.4°C 1 d after. From that day on, the average air temperature increased to 28.7°C at the end of the selected period. As can be seen in Figure 7b, the average daily relative humidity was 0.31 before and 0.51 after rainfalls, followed by a 3 d gradual decrease to 0.14, with a slight increase on the final day to 0.21. As is seen in Figure 7e, the atmospheric pressure followed the same variation pattern as the relative humidity did. The daily average atmospheric pressure was 87528.8 *Pa* before and 87907.2 *Pa* after the precipitation. From the second day onwards, the average atmospheric pressure first decreased to 86791.3 *Pa* on the fifth day, and then increased again to 86753.21 *Pa* on the last day.

[44] Following *van de Griend and Owe* [1994], the aerodynamic resistance (r_a) and soil surface resistance (r_s) was expressed as

$$r_a = \frac{1}{k^2 U}\left[\ln\left(\frac{z_m - d - z_{om}}{z_{om}}\right) - \psi_{sm}\right]\left[\ln\left(\frac{z_m - d - z_{oh}}{z_{oh}}\right) - \psi_{sh}\right],$$
$$r_s = r_{sl} e^{a(\theta_{\min} - \theta_{sur})} \tag{18}$$

where k is the von Karman constant (=0.41); U(m s^{-1}) the measured wind speed at certain height; Z_m(m) the height of wind speed measurement; d (m) the zero plane displacement (=0 for bare soil); Z_{om} (=0.001 m) the surface roughness length for momentum flux; ψ_{sm} the atmospheric stability correction factor for momentum flux; Z_{oh} (= 0.001 m) the surface roughness length for heat flux; ψ_{sh} the atmospheric stability correction factor for heat flux; r_{sl}(=10 s m^{-1}) the resistance to molecular diffusion across the water surface itself; a (=35.63) the fitted parameter; $\theta_{\min}$ (= 0.15 m^{-3} m^3) the empirical minimum value above which the soil is able to deliver vapor at a potential rate; and θ_{sur} the soil water content in the topsoil layer.

3.3.3. Model Validation

[45] The field measurements of soil moisture and temperature described by *Zeng et al.* [2009], were used to validate the proposed model. The soil temperature was measured at

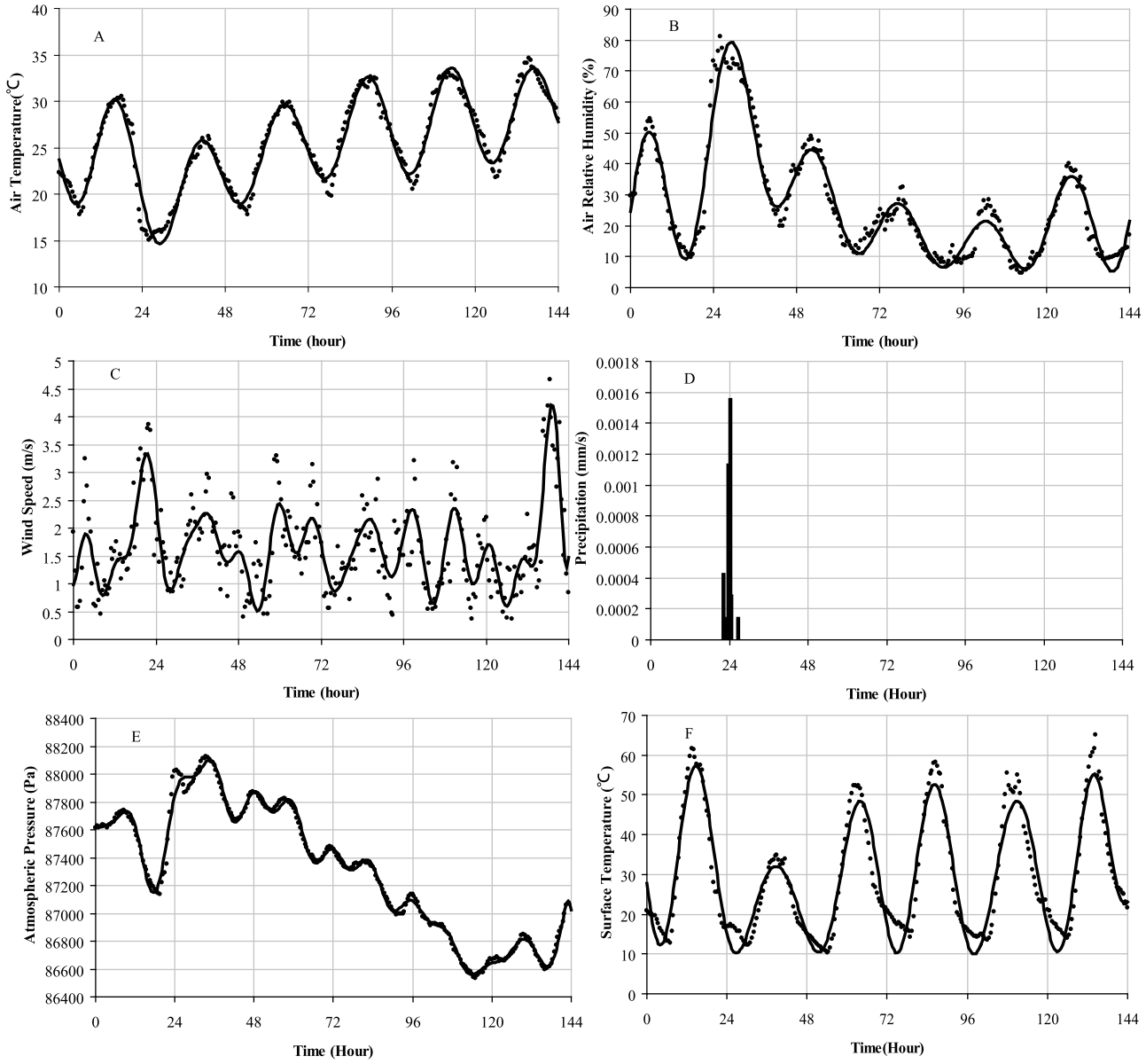

Figure 7. Diurnal changes in meteorological variables: (a) air temperature, (b) relative humidity, (c) wind speed, (d) precipitation, (e) atmospheric pressure, and (f) surface temperature. They are recorded every 30 min from 13 to 19 June 2008. The solid lines are the approximation and the dots are the measurement.

depths of 2, 5, 10, 20 and 50 cm by soil temperature profile sensor (STP01, Hukseflux Thermal Sensors B.V., Delft, Netherlands). According to Figure 8, there was reasonably good agreement between simulated and measured soil temperatures at different depths. The simulation matched the diurnal variations on most days. The underestimation occurring at 2 cm depth during the whole simulation period should partially be attributed to the Fourier-transformed surface temperature in Figure 7f. There were overestimations at other depths on some days. For example, overestimation occurred on day 1 at depths of 10, 20 and 50 cm, and on day 5 and 6 at depths of 10 and 20 cm. The simulations of temperature with and without considering airflow were compared in Figure 8. At the selected depths, there is no big difference between the two models. The root mean square errors (RMSEs) between the simulation (considering airflow) and the measurement are 4.135°C, 3.047°C, 3.667°C, 3.559°C and 1.532°C at the depth of 2, 5, 10, 20 and 50 cm, respectively. For the simulation without considering airflow, the RMSEs are 4.131°C, 3.031°C, 3.572°C, 3.394°C and 1.541°C at the selected depths.

[46] The soil moisture was measured at a depth of 10, 20, 30, 40, and of 50 cm by soil water content profile sensor (EasyAG50, Sentek Pty. Ltd., Stepny, Australia). The quality of soil moisture measurement was quantitatively assessed and calibrated by *Zeng et al.* [2009]. A major concern with measuring soil moisture in sand was the temperature effect. The temperature had an effect on readings of the moisture sensors of 14.4% between 12°C and 45°C at 10 cm, of 13.9% between 11°C and 50°C at 20 cm, of 14% between 9°C and

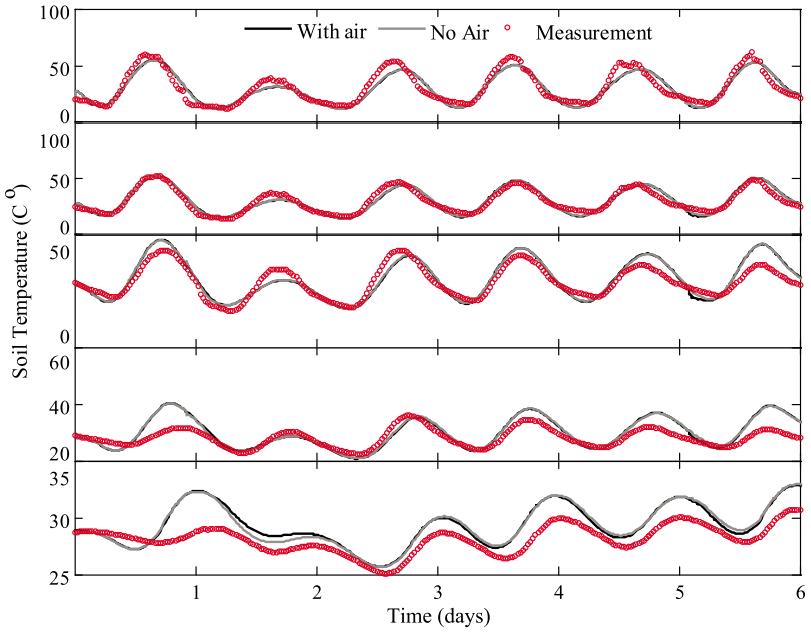

Figure 8. Comparison between simulated (i.e., by model with and without considering airflow) and measured soil temperature during 13–19 June 2008, at selected depths: (top to bottom) 2 cm, 5 cm, 10 cm, 20 cm and 50 cm. The solid black line is the simulation with airflow, the solid gray line is the simulation without airflow, and the red open circle is the measurement.

51°C at 30 cm, of 13% between 9°C and 55°C at 40 cm, and of 15% between 8°C and 55°C at 50 cm. After calibration, the temperature effects at the depths of 10, 20, 30, 40, and 50 cm were reduced by 92%, 93%, 93.8%, 88%, and 82%, respectively [*Zeng et al.*, 2009]. This ensured the quality of the measurements used to assess the model performance in simulating soil moisture variations.

[47] While the temperature simulation was in close agreement with the measurements, the soil moisture simulation was not, except for the depths of 10 cm and 50 cm (Figure 9). At a depth of 10 cm, the simulation captured the important trend, which was the response of soil moisture to the precipitation at the end of day 1. However, the measurements at depths 20, 30 and 40 cm did not follow the

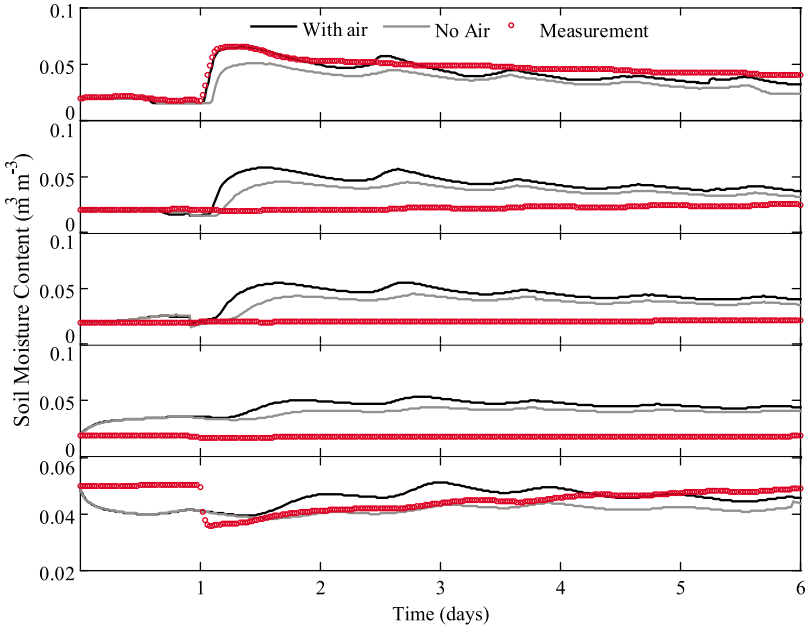

Figure 9. Same as Figure 8 but for soil moisture content at selected depths: (top to bottom) 10 cm, 20 cm, 30 cm, 40 cm and 50 cm. The solid black line is the simulation with airflow, the solid gray line is the simulation without airflow, and the red open circle is the measurement.

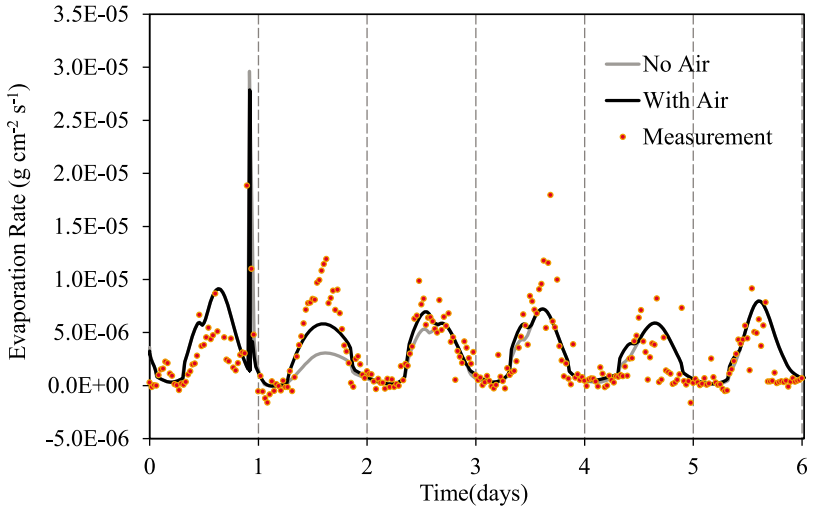

Figure 10. Comparison between simulated evaporation rates and actual measurements from 13 to 19 June 2008.

same trend as the simulation. This partially indicated that the parameters in soil hydraulic properties, assumed vertically homogeneous, were probably not correct. HYDRUS1D [*Saito et al.*, 2006] was also used to simulate soil moisture and temperature variations. Results of this showed that agreement between measured and modeled soil moisture content was not achieved throughout the profile [*Zeng et al.*, 2009]. Further investigation should be undertaken to quantify the heterogeneity of the sand at the field site.

[48] Figure 9 shows also the simulation of soil water content without considering airflow. Compared to Figure 8, the discrepancy between the two models in simulating soil water content is more obvious. The RMSEs between the simulated (considering airflow) and the measured volumetric soil water content are 0.0052, 0.0218, 0.0232, 0.0268 and 0.0051 (m^{-3} m^3) at the depth of 10, 20, 30, 40 and 50 cm. For the simulation without considering airflow, the RMSEs are 0.0189, 0.0089, 0.0114, 0.018 and 0.0068 (m^{-3} m^3) at the selected depths. Except for the depth of 20, 30 and 40 cm, the model considering airflow performs closer to the field measurement than without airflow. However, at these less-good-match depths, the model with airflow does have a much more sensitive response to the rainfall event than without considering airflow. Even at the depth of 50 cm, clear response to the rainfall event is shown by the model with airflow, while not by the model without considering airflow.

3.3.4. Comparisons With Evaporation Measurement

[49] With boundary conditions and forcing data in place, the validated model was used to determine the surface evaporative flux, a crucial parameter subsequently affecting the atmospheric modeling. The observed evaporative flux was calculated from the latent heat flux recorded by a three-dimensional eddy covariance system (Campbell Scientific, Inc., Logan, UT) installed 2 m above the surface. The system consisted of a CSAT3 three-dimensional sonic anemometer and a KH20 krypton hygrometer. The CSAT3 measured wind speed in three dimensions at a frequency of 10 Hz, and with the same frequency the KH20 measured vapor pressure. With the high-frequency data from CSAT3 and KH20, the latent heat flux was obtained every 30 min. The sensible heat flux was also obtained by the eddy covariance system.

[50] Figure 10 shows the comparison between evaporation rates, calculated by the proposed model and the model excluding airflow (e.g., PdV model), and the actual measurements. The normalized root mean squared deviation (NRMSD) was used to quantify the simulation's goodness of fit. NRMSD was expressed as percentage, where lower values indicated better agreement between simulation and measurement.

[51] Except for the day immediately after rainfall (the second day), there was no big difference in the calculated evaporation rate, whether airflow was included or not. The NRMSDs for the selected simulation period were 13% and 14% for the proposed model and the no-air model, respectively. However, if only the second day was taken into account, the NRMSD of the proposed model was 16% and that of the no-air model 27%. This meant that in this field case the proposed model did improve the simulation and made it come closer to reality than the no-air model did. The significant improvement seen on the second day was mainly attributed to the moist soil immediately after the rainfall event. During the rest of the simulation period, the topsoil layer dried up, diminishing the advantage of including the airflow mechanism.

4. Conclusions

4.1. Summary of Numerical Results

[52] A physics-based approach was adopted to develop a theoretical equation system for coupling liquid, water vapor, dry air and heat transfer in unsaturated soil, considering water vapor diffusion, advection and dispersion. On the basis of previous work by *Milly* [1982], who analyzed the simultaneous mass and heat transfer under constant air pressure, a fully coupled model was developed, in which dry air was treated as a single phase. Thus, not only diffusion, but also convection and dispersion were included in the vapor transport mechanism. The treatment also included atmospheric pressure, acting as the driving force gradient for

the liquid transport and advective flux, conveyed by the dry air flux, in the energy balance calculation.

[53] The three partial differential equations of the proposed model, based on the state variables of matric potential, temperature and air pressure, were solved numerically using a combination of a finite element method for spatial discretization and a finite difference method for temporal discretization. The model was verified by testing its capacity to describe the physical processes involved in the isothermal two-phase flow and the coupled moisture and heat transfer. Excellent agreement was achieved between the proposed model and the published experimental and numerical studies.

[54] On the basis of literature studies (the cases of Milly, and Touma and Vauclin), the fully coupled problem was investigated by introducing heat flow into the isothermal two-phase flow and dry airflow into the coupled moisture and heat flow. The results showed that in a very dry soil, airflow had a significant influence on the water vapor transfer. In a bounded soil column, 10 cm thick, the water vapor transfer was retarded because of the outward air pressure gradient. In the transient infiltration experiments, the simulation results showed that when the air effect was significant (i.e., in a bounded soil column), the inclusion of heat flow increased the infiltration process (Figure 6a). However, the heat flow did not affect the two-phase flow (air-water flow) noteworthy when the bottom of the column was opened. In that case, the soil air pressure equilibrated quickly with the atmospheric pressure. In the bounded column, where the air phase played a significant role in the water phase flow, the effect of the heat flow was outstanding. The thermal gradient driving forces partially pushed the water supposed to be stored at certain depth, down and made the water content profiles more abrupt.

[55] The proposed model was then applied to a field case, in which soil moisture, temperature and evaporation rate were measured. With the boundary conditions and the atmospheric forcing, the model generated good agreement between simulated and measured soil temperature. However, the comparison with measured soil moisture indicated that the parameters in soil hydraulic properties, assumed vertically homogeneous, were likely not correct. Further investigation is needed to quantify the heterogeneity of the sand in the field site. The comparison between the measured and the simulated evaporation rates, by both the proposed model and the no-air model, demonstrated that the proposed model did improve the simulation of evaporation and made it come closer to reality.

4.2. Is it Necessary to Consider Airflow in LSMs?

[56] As mentioned previously, most of the land surface models (LSMs) do not consider two-phase flows. Soil water dynamics remain highly simplified in the LSMs, even though they have evolved from first generation to third generation [*Sellers et al.*, 1997]. This simplification has resulted in the transforming of soil moisture into an index used for calculating evapotranspiration and runoff, rather than representing the actual mass of moisture in the soil [*Robock et al.*, 1998]. This has lead to poor simulation of soil moisture dynamics in extremely dry environments [*Walker et al.*, 2001a], such as deserts. The invalidity of this simplification has contributed to the lack of realistic physical coupling between soil moisture and temperature. Only the diffusivity forms of the conservation equations for soil moisture and temperature are used in the LSMs [*Shao and Henderson-Sellers*, 1996a]. The coupled moisture and heat transfer model has hardly been used to retrieve soil moisture profiles with a data assimilation technique, though it has been proven to be successful [*Walker et al.*, 2001b]. Furthermore, there are very few studies tackling the inclusion of atmospheric pressure in the LSMs based on a two-phase flow approach.

[57] In fact, atmospheric pressure variation (e.g., from 86535 *Pa* to 88123 *Pa* in the field case) can dynamically move water vapor and dry air in and out of soil [*Tillman and Smith*, 2005]. The discussion in section 3 shows that airflow is actually strongly coupled to simultaneous moisture and heat transport in the soil. When compared to measured evaporation, the model including airflow mechanisms did improve the simulation of evaporation and made it come closer to reality. On the day immediately after a rainfall event, the effect of including airflow was significant and showed an underestimation error of 33% where airflow was neglected. It is clear that the coupled liquid, water vapor, dry air and heat transport mechanism (i.e., simultaneous moisture and heat transport including airflow) should be considered in LSMs.

[58] One note on the additional computational cost required to include the airflow would be practical here. With a dual core processor (Intel(R), Core(TM) 2 CPU 6400@ 2.13 GHz, 2.13 GHz), an installed memory (RAM, 2GB), and a 32 bit system operating with Windows 7 (service pack 1, Copyright©2009 Microsoft Corporation), the computational cost of the proposed model was 58.2 s, compared to 48.7 s for the no-air model, in the field case used in this study. Thus, the computational costs for the proposed model were 19.5% higher than for the model without considering airflow.

4.3. Limitations and Future Work

[59] This study only discussed the necessity of considering two-phase flow mechanisms in LSMs from a subsurface physical point of view. The incorporation of the proposed model into a LSM was not implemented. The main purpose was to demonstrate how a complex model (two-phase heat and mass flow model) can be developed from a relative simple model (PdV model), and how important a role the additional complexity can play in the model performance. Section 2 shows the development of the proposed complex model, and its value is demonstrated by comparisons between the proposed model and the simple model with the real atmospheric forcing and evaporation measurement (section 3.3).

[60] It is clear that the proposed model lacks the inclusion of freezing and thawing processes, where frozen soil can impede water infiltration and influence the hydrological cycle [*Bayard et al.*, 2005], and soil thaw can enhance soil-atmosphere gas exchanges [*Goulden et al.*, 1998; *Schuur et al.*, 2009]. In the near future, NASA's Soil Moisture Active and Passive (SMAP) mission will be launched for mapping soil moisture and freeze/thaw state. To not only include the airflow mechanism discussed above, but also assimilate these extra satellite data, a land model considering the freezing/thawing process should be developed, extending beyond the focus of this research.

[61] It is also necessary to quantify the capabilities of the proposed model to handle more complex and realistic situations, such as the acceleration in the infiltration process

due to a considerable volume of CO_2 in the soil. It would also be interesting to test the proposed model with more experimental data in a desert environment, in order to gain understanding about the moisture transport mechanism in a desert ecosystem, as no satisfactory explanation exists to date for such an ecosystem on soil water trapped at certain depths below the surface [*Zeng et al.*, 2009]. In situ experiments measuring air pressure in the soil and the atmosphere would also help to gain insight in the parameterization schemes of the proposed model.

Appendix A: Parameterizations

[62] These parameterization equations link the independent variables (soil matric potential, soil temperature and soil air pressure) and the dependent variables (i.e., volumetric water content, vapor density, etc.). Each governing equation is solved for a single unknown, for example, equations (1) with (3) for soil matric potential, equations (4) with (5) for soil air pressure and equation (6) for soil temperature. The closure of the model developed above requires all dependent variables to be computable from the set of independent variables. The governing equations are finally written in terms of the independent variables when the parameterizations given below are substituted.

A1. Gas-Phase Density

A1.1. Water Vapor Density

[63] Water vapor density, ρ_V, is evaluated as determined by *Philip and De Vries* [1957]

$$\rho_V = \rho_{sV} H_r; \text{with } H_r = \exp\left(hg/R_V T\right); \text{and}$$
$$\rho_{sV} = \frac{10^{-3}}{T}\exp\left(31.3716 - \frac{6014.79}{T} - 7.92495\times 10^{-3} T\right) \quad \text{(A1)}$$

where ρ_{sV}(kg m^{-3}) is the density of saturated water vapor [*Saito et al.*, 2006]; H_r the relative humidity; R_V(461.5 J kg^{-1} K^{-1}) the specific gas constant for water vapor; g(m s^{-2}) the gravitational acceleration; and T(K) the temperature. The vertical gradient of the water vapor density can be expressed as

$$\frac{\partial \rho_V}{\partial z} = \rho_{sV}\frac{\partial H_r}{\partial T}|_h \frac{\partial T}{\partial z} + \rho_{sV}\frac{\partial H_r}{\partial h}|_T \frac{\partial h}{\partial z} + H_r \frac{\partial \rho_{sV}}{\partial T}\frac{\partial T}{\partial z} \quad \text{(A2)}$$

A1.2. Dry Air Density [*Thomas and Sansom*, 1995]

[64] Assuming that pore-air and pore-vapor may be considered to be ideal gas, dry air and water vapor density can be expressed as

$$\rho_{da} = \frac{P_{da}}{R_{da}T}, \text{and } \rho_V = \frac{P_V}{R_V T} \quad \text{(A3)}$$

where R_{da}(=287.1 J kg^{-1} K^{-1}) is the specific gas constant for dry air; P_{da}(Pa) and P_V(Pa) are dry air pressure and water vapor pressure, respectively; and T(K) the soil temperature. According to Dalton's law of partial pressure, the mixed soil air pressure (P_g) should be equal to the sum of the dry air pressure and the water vapor pressure

$$P_g = P_{da} + P_v \quad \text{(A4)}$$

The dry air density may then be rewritten as

$$\rho_{da} = \frac{P_g}{R_{da}T} - \frac{\rho_V R_V}{R_{da}} \quad \text{(A5)}$$

Differentiating equation (A5) with respect to time (t) and space (z) yields

$$\frac{\partial \rho_{da}}{\partial t} = X_{aa}\frac{\partial P_g}{\partial t} + X_{aT}\frac{\partial T}{\partial t} + X_{ah}\frac{\partial h}{\partial t}$$
$$\frac{\partial \rho_{da}}{\partial z} = X_{aa}\frac{\partial P_g}{\partial z} + X_{aT}\frac{\partial T}{\partial z} + X_{ah}\frac{\partial h}{\partial z} \quad \text{(A6)}$$

where

$$X_{aa} = \frac{1}{R_{da}T}; X_{aT} = -\left[\frac{P_g}{R_{da}T^2} + \frac{R_V}{R_{da}}\left(H_r\frac{\partial \rho_{sV}}{\partial T} - \frac{\rho_{sV} hg H_r}{R_V T^2}\right)\right];$$
$$\text{and } X_{ah} = -\frac{\rho_{sV} g H_r}{R_{da}T} \quad \text{(A7)}$$

A2. Permeability

[65] The pore size distribution model of *Mualem* [1976] was used to predict the isothermal hydraulic conductivity, K_{Lh}, from the saturated hydraulic conductivity [*van Genuchten*, 1980]:

$$K_{Lh} = K_s K_{rh} = K_s S_e^l\left[1 - \left(1 - S_e^{1/m}\right)^m\right]^2 \quad \text{(A8)}$$

where K_s(m s^{-1}) is the saturated hydraulic conductivity; K_{rh} the relative hydraulic conductivity; S_e the effective saturation (unitless, $S_e = (\theta - \theta_{res})/(\theta_{sat} - \theta_{res})$); θ_{res} the residual water contents; and l and m are empirical parameters. Of these parameters, $l = 0.5$, and m can be expressed as $m = 1–1/n$, which in turn could be determined by fitting Van Genuchten's analytical model [*van Genuchten*, 1980]

$$\theta(h) = \begin{cases} \theta_{res} + \dfrac{\theta_{sat} - \theta_{res}}{[1 + |\alpha h|^n]^m}, & h < 0 \\ \theta_{sat}, & h \geq 0 \end{cases} \quad \text{(A9)}$$

where α(m^{-1}) is related to the inverse of the air entry pressure, and n is a measure of the pore size distribution.

[66] Taking the temperature dependence of matric pressure into consideration [*Nimmo and Miller*, 1986; *Nassar and Horton*, 1989; *Noborio et al.*, 1996], the thermal hydraulic conductivity, K_{LT}, is defined as

$$K_{LT} = K_{Lh}\left(hG_{wT}\frac{1}{\gamma_0}\frac{d\gamma}{dT}\right) \quad \text{(A10)}$$

where G_{wT} is the gain factor (dimensionless), that assesses the temperature dependence of the surface tension of soil water; γ(g s^{-2}) is the surface tension of soil water; and γ_0(= 71.89 g s^{-2}) the surface tension at 25°C. The temperature dependence of γ is given by *Saito et al.* [2006]

$$\gamma = 75.6 - 0.1425T - 2.38\times 10^{-4} T^2 \quad \text{(A11)}$$

where T(°C) is the temperature.

[67] According to *Scanlon* [2000], the intrinsic permeability of a media may be defined as

$$k_g = \frac{K_s \mu_w}{\rho_L g} \tag{A12}$$

where μ_w(kg m^{-1} s^{-1}) is the dynamic viscosity of water.

A3. Dynamic Viscosity

[68] The dynamic viscosity of water given by *Fogel'son and Likhachev* [2000] is

$$\mu_w = \mu_{w0} \exp[\mu_1/(R \cdot (T + 133.3)] \tag{A13}$$

where $\mu_{w0} = 2.4152 \times 10^{-5}$ (Pa s), $\mu_1 = 4.7428$ (kJ mol^{-1}), R = 8.314472 (J mol^{-1}°C^{-1}), and T(°C) is the temperature.

A4. Transport Coefficient for Thermal Adsorbed Liquid Flow

[69] According to *Groenevelt and Kay* [1974], the transport coefficient for adsorbed liquid flow due to temperature gradient may be expressed as:

$$D_{TD} = \frac{H_w \varepsilon}{b f_0 \mu_w (T + 273.15)} \left(1.5548 \cdot 10^{-17}\right) \tag{A14}$$

where Hw(J m^{-2}) is the integral heat of wetting; b = 4×10^{-8} (m); T(°C) is the temperature; and f_0 is the tortuosity factor, which may be expressed as [*Millington and Quirk*, 1961]

$$f_0 = \theta_a^{7/3}/\theta_{sat}^2 \tag{A15}$$

A5. Diffusion and Dispersion Coefficients

[70] Following *Milly and Eagleson* [1980], the water vapor diffusivity in soil, D_e, is defined as

$$D_e = f_0 \theta_a D_a \tag{A16}$$

where D_a(m^2 s^{-1}) is the diffusivity of water vapor in air at temperature T (K) [*Saito et al.*, 2006]:

$$D_a = 2.12 \times 10^{-5} \left(\frac{T}{273.15}\right)^2 \tag{A17}$$

Following the liquid island concept of *Philip and De Vries* [1957], a well-known enhancement factor is derived by *Cass et al.* [1984] to account for the increase in thermal water vapor flux, which is expressed as

$$\eta = 9.5 + 3 \cdot \theta/\theta_{sat} - 8.5 \cdot \exp\left\{-\left[\left(1 + 2.6/\sqrt{f_c}\right)\theta/\theta_{sat}\right]^4\right\} \tag{A18}$$

where f_c is the mass fraction of clay in sand (0.02); and θ_{sat} the saturated water content. The variable η only appears in the water vapor diffusion term associated with the temperature gradient in the form of $D_e \eta \frac{\partial \rho_V}{\partial T} \frac{\partial T}{\partial z}$.

[71] The gas phase longitudinal dispersion coefficient, D_{Vg}, was estimated by *Bear* [1972] as

$$D_{Vg} = \alpha_{Li} \cdot q_i (i = gas, liquid) \tag{A19}$$

where q_i is the pore fluid flux in phase i; and α_{Li}(m), the longitudinal dispersivity in phase i, has been evaluated by various authors for different levels of soil saturation. Laboratory studies have shown that α_{Li} increases when the soil volumetric water content decreases. In this work, as in the work of *Grifoll et al.* [2005], a correlation made from simulation results by *Sahimi et al.* [1986] and experimental data obtained by *Haga et al.* [1999] was used:

$$\alpha_{Li} = \alpha_{Li\_sat} \cdot \left[13.6 - 16 \cdot (\theta_a/\varepsilon) + 3.4 \cdot (\theta_a/\varepsilon)^5\right] \tag{A20}$$

As *Grifoll et al.* [2005] pointed out, because of the lack of dispersivity values, the saturation dispersivity, α_{Li_sat}, used in the above correlation was taken to be 0.078 m, as reported in the field experiments of *Biggar and Nielsen* [1976] and shown to be a reasonable value in previous modeling studies [*Cohen and Ryan*, 1989].

A6. Thermal Conductivity, Heat of Wetting, and Latent Heat

[72] The coefficient of thermal conductivity of unsaturated soil combines the thermal conductivity of solid particles, liquid and dry air in the absence of flow and is expressed by *Chung and Horton* [1987] as

$$\lambda_{eff} \approx b_1 + b_2\theta + b_3\theta^{0.5} \tag{A21}$$

where b_1, b_2, and b_3 are empirical regression parameters that have three sets of values for clay (−0.197, −0.962 and 2.521), loam (0.243, 0.393 and 1.534) and sand (0.228, −2.406 and 4.909), respectively.

[73] The differential heat of wetting, W(J Kg^{-1}), is the amount of heat released when a small amount of free water is added to the soil matrix and is expressed by *Prunty* [2002] as

$$W = -0.002932h \tag{A22}$$

where h is in m.

[74] According to *Saito et al.* [2006], the latent heat of vaporization varies with T(°C) as

$$L(T) = L_0 - (c_L - c_V)(T - T_r) \approx 2.501 \times 10^6 - 2369.2T \tag{A23}$$

[75] **Acknowledgments.** The research projects on which this paper is based were funded by "The ESA-MOST Dragon Programme" and by the European Commission (Call FP7-ENV-2007-1 Grant nr. 212921) as part of the CEOP – AEGIS project (http://www.ceop-aegis.org/) coordinated by the Université Louis Pasteur (and supported by the Fundamental Research Funds for the Central Universities). We thank the anonymous referees for their helpful and constructive comments and suggestions for improving the manuscript.

References

Ataie-Ashtiani, A., and D. Raeesi-Ardekani (2010), Comparison of numerical formulations for two-phase flow in porous media, *Geotech. Geol. Eng.*, *28*(4), 373–389, doi:10.1007/s10706-009-9298-4.

Avissar, R. (1992), Conceptual aspects of a statistical-dynamic approach to represent landscape subgrid-scale heterogeneities in atmospheric models, *J. Geophys. Res.*, *97*(D3), 2729–2742.

Avissar, R., and R. A. Pielke (1989), A parameterization of heterogeneous land surfaces for atmospheric numerical models and its impact on regional

meteorology, *Mon. Weather Rev.*, *117*(10), 2113–2136, doi:10.1175/1520-0493(1989)117<2113:APOHLS>2.0.CO;2.

Balsamo, G., P. Viterbo, A. Beljaars, B. van den Hurk, M. Hirschi, A. K. Betts, and K. Scipal (2009), A revised hydrology for the ECMWF model: Verification from field site to terrestrial water storage and impact in the integrated forecast system, *J. Hydrometeorol.*, *10*(3), 623–643, doi:10.1175/2008JHM1068.1.

Bastidas, L. A., T. S. Hogue, S. Sorooshian, H. V. Gupta, and W. J. Shuttleworth (2006), Parameter sensitivity analysis for different complexity land surface models using multicriteria methods, *J. Geophys. Res.*, *111*, D20101, doi:10.1029/2005JD006377.

Bayard, D., M. Stahli, A. Parriaux, and H. Fluhler (2005), The influence of seasonally frozen soil on the snowmelt runoff at two Alpine sites in southern Switzerland, *J. Hydrol.*, *309*, 66–84, doi:10.1016/j.jhydrol.2004.11.012.

Bear, J. (1972), *Dynamics of Fluid in Porous Media*, Dover, Mineola, N Y.

Biggar, J. W., and D. R. Nielsen (1976), Spatial variability of the leaching characteristics of a field soil, *Water Resour. Res.*, *12*(1), 78–84, doi:10.1029/WR012i001p00078.

Braud, I., A. C. Dantasantonino, M. Vauclin, J. L. Thony, and P. Ruelle (1995), A simple soil-plant-atmosphere transfer model (SISPAT) development and field verification, *J. Hydrol.*, *166*(3–4), 213–250, doi:10.1016/0022-1694(94)05085-C.

Buckingham, E. (1904), Contributions to our knowledge of aeration of soils, *Bull. 25*, Bur. of Soils, U.S. Dep. of Agric., Washington, D. C.

Camillo, P. J., and R. J. Gurney (1986), A resistance parameter for bare-soil evaporation models, *Soil Sci.*, *141*(2), 95–105, doi:10.1097/00010694-198602000-00001.

Cass, A., G. S. Campbell, and T. L. Jones (1984), Enhancement of thermal water vapor diffusion in soil, *Soil Sci. Soc. Am. J.*, *48*, 25–32, doi:10.2136/sssaj1984.03615995004800010005x.

Celia, M. A., and P. Binning (1992), A mass conservative numerical solution for two-phase flow in porous media with application to unsaturated flow, *Water Resour. Res.*, *28*(10), 2819–2828, doi:10.1029/92WR01488.

Celia, M. A., and J. M. Nordbotten (2009), Practical modeling approaches for geological storage of carbon dioxide, *Ground Water*, *47*(5), 627–638, doi:10.1111/j.1745-6584.2009.00590.x.

Celia, M. A., H. Rajaram, and L. A. Ferrand (1993), A multi-scale computational model for multiphase flow in porous media, *Adv. Water Resour.*, *16*(1), 81–92, doi:10.1016/0309-1708(93)90031-A.

Chung, S. O., and R. Horton (1987), Soil heat and water flow with a partial surface mulch, *Water Resour. Res.*, *23*(12), 2175–2186, doi:10.1029/WR023i012p02175.

Cohen, Y., and P. A. Ryan (1989), Chemical transport in the top soil zone—The role of moisture and temperature gradients, *J. Hazard. Mater.*, *22*(3), 283–304, doi:10.1016/0304-3894(89)80002-0.

de Rooij, G. H. (2010), Comments on "Improving the numerical simulation of soil moisture-based Richards equation for land models with a deep or shallow water table," *J. Hydrometeorol.*, *11*(4), 1044–1050, doi:10.1175/2010JHM1189.1.

Desborough, C. E. (1999), Surface energy balance complexity in GCM land surface models, *Clim. Dyn.*, *15*(5), 389–403, doi:10.1007/s003820050289.

deVries, D. A. (1958), Simultaneous transfer of heat and moisture in porous media, *Eos Trans. AGU*, *39*(5), 909–916.

Dirmeyer, P. A., Z. C. Guo, and X. Gao (2004), Comparison, validation, and transferability of eight multiyear global soil wetness products, *J. Hydrometeorol.*, *5*(6), 1011–1033, doi:10.1175/JHM-388.1.

Dirmeyer, P. A., X. A. Gao, M. Zhao, Z. C. Guo, T. K. Oki, and N. Hanasaki (2006), GSWP-2: Multimodel analysis and implications for our perception of the land surface, *Bull. Am. Meteorol. Soc.*, *87*(10), 1381–1397, doi:10.1175/BAMS-87-10-1381.

Dong, J. R., G. D. Salvucci, and R. B. Myneni (2001), Improving the precision of simulated hydrologic fluxes in land surface models, *J. Geophys. Res.*, *106*(D13), 14,357–14,368, doi:10.1029/2001JD900126.

Ek, M. B., K. E. Mitchell, Y. Lin, E. Rogers, P. Grunmann, V. Koren, G. Gayno, and J. D. Tarpley (2003), Implementation of Noah land surface model advances in the National Centers for Environmental Prediction operational mesoscale Eta model, *J. Geophys. Res.*, *108*(D22), 8851, doi:10.1029/2002JD003296.

Fayer, M. J. (2000), UNSAT-H Version 3.0: Unsaturated soil water and heat flow model-theory, user manual, and examples, *PNNL-13249*, 184 pp., NTIS, Springfield, Va.

Flerchinger, G. N. (2000), The simultaneous heat and water (SHAW) model: Technical documentation, *Tech. Rep. NWRC 2000-09*, USDA Agric. Res. Serv., Boise, Idaho.

Flerchinger, G. N., and K. E. Saxton (1989), Simultaneous heat and water model of a freezing snow-residue-soil system. 1. Theory and development, *Trans. Am. Soc. Agric. Eng.*, *32*(2), 565–571.

Fogel'son, R. L., and E. R. Likhachev (2000), Temperature dependence of diffusion coefficient, *Phys. Met. Metalloved.*, *90*(1), 58–61.

Gates, J. B., W. M. Edmunds, J. Z. Ma, and B. R. Scanlon (2008), Estimating groundwater recharge in a cold desert environment in northern China using chloride, *Hydrogeol. J.*, *16*(5), 893–910, doi:10.1007/s10040-007-0264-z.

Goulden, M. L., et al. (1998), Sensitivity of Boreal forest carbon balance to soil thaw, *Science*, *279*, 214–217, doi:10.1126/science.279.5348.214.

Grifoll, J., J. M. Gast, and Y. Cohen (2005), Non-isothermal soil water transport and evaporation, *Adv. Water Resour.*, *28*, 1254–1266, doi:10.1016/j.advwatres.2005.04.008.

Groenevelt, P. H., and B. D. Kay (1974), On the interaction of water and heat transport in frozen and unfrozen soils: II. The liquid phase, *Soil Sci. Soc. Am. Proc.*, *38*, 400–404, doi:10.2136/sssaj1974.03615995003800030012x.

Gupta, H. V., L. A. Bastidas, S. Sorooshian, W. J. Shuttleworth, and Z. L. Yang (1999), Parameter estimation of a land surface scheme using multicriteria methods, *J. Geophys. Res.*, *104*(D16), 19,491–19,503, doi:10.1029/1999JD900154.

Haga, D., Y. Niibori, and T. Chida (1999), Hydrodynamic dispersion and mass transfer in unsaturated flow, *Water Resour. Res.*, *35*(4), 1065–1077, doi:10.1029/1998WR900111.

Haverkamp, R., M. Vauclin, J. Touma, P. J. Wierenga, and G. Vachaud (1977), A comparison of numerical simulation models for one-dimensional infiltration, *Soil Sci. Soc. Am. J.*, *41*(2), 285–294, doi:10.2136/sssaj1977.03615995004100020024x.

Henderson-Sellers, A., Z. L. Yang, and R. E. Dickinson (1993), The Project for Intercomparison of Land-Surface Parameterization Schemes, *Bull. Am. Meteorol. Soc.*, *74*(7), 1335–1349, doi:10.1175/1520-0477(1993)074<1335:TPFIOL>2.0.CO;2.

Hogue, T. S., L. A. Bastidas, H. V. Gupta, and S. Sorooshian (2006), Evaluating model performance and parameter behavior for varying levels of land surface model complexity, *Water Resour. Res.*, *42*, W08430, doi:10.1029/2005WR004440.

Jassal, R. S., M. D. Novak, and T. A. Black (2003), Effect of surface layer thickness on simultaneous transport of heat and water in a bare soil and its implications for land surface schemes, *Atmos. Ocean*, *41*(4), 259–272, doi:10.3137/ao.410401.

Kato, H., M. Rodell, F. Beyrich, H. Cleugh, E. van Gorsel, H. Z. Liu, and T. P. Meyers (2007), Sensitivity of land surface simulations to model physics, land characteristics, and forcings, at four CEOP sites, *J. Meteorol. Soc. Jpn.*, *85A*, 187–204, doi:10.2151/jmsj.85A.187.

Koster, R. D., T. Oki, and M. J. Suarez (1999), The offline validation of land surface models: Assessing success at the annual timescale, *J. Meteorol. Soc. Jpn.*, *77*(1B), 257–263.

Koster, R. D., Z. C. Guo, R. Q. Yang, P. A. Dirmeyer, K. Mitchell, and M. J. Puma (2009), On the nature of soil moisture in land surface models, *J. Clim.*, *22*(16), 4322–4335, doi:10.1175/2009JCLI2832.1.

Massman, W. J. (2006), Advective transport of CO_2 in permeable media induced by atmospheric pressure fluctuations: 1. An analytical model, *J. Geophys. Res.*, *111*, G03004, doi:10.1029/2006JG000163.

Miguez-Macho, G., Y. Fan, C. P. Weaver, R. Walko, and A. Robock (2007), Incorporating water table dynamics in climate modeling: 2. Formulation, validation, and soil moisture simulation, *J. Geophys. Res.*, *112*, D13108, doi:10.1029/2006JD008112.

Millington, R. J., and J. P. Quirk (1961), Permeability of porous solids, *Trans. Faraday Soc.*, *57*, 1200–1207, doi:10.1039/tf9615701200.

Milly, P. C. (1982), Moisture and heat transport in hysteretic, inhomogeneous porous media: A matric head-based formulation and a numerical model, *Water Resour. Res.*, *18*(3), 489–498, doi:10.1029/WR018i003p00489.

Milly, P. C. D., and P. S. Eagleson (1980), The coupled transport of water and heat in a vertical soil column under atmospheric excitation, M.S. thesis, Dep. of Civ. Eng., Mass. Inst. of Technol., Cambridge.

Mualem, Y. (1976), A new model for predicting the hydraulic conductivity of unsaturated porous media, *Water Resour. Res.*, *12*(3), 513–522, doi:10.1029/WR012i003p00513.

Nassar, I. N., and R. Horton (1989), Water transport in unsaturated nonisothermal salty soil. II: Theoretical development, *Soil Sci. Soc. Am. J.*, *53*(5), 1330–1337, doi:10.2136/sssaj1989.03615995005300050005x.

Nimmo, J. R., and E. E. Miller (1986), The temperature dependence of isothermal moisture vs. potential characteristics of soils, *Soil Sci. Soc. Am. J.*, *50*, 1105–1113, doi:10.2136/sssaj1986.03615995005000050004x.

Niu, G. Y., Z. L. Yang, R. E. Dickinson, L. E. Gulden, and H. Su (2007), Development of a simple groundwater model for use in climate models and evaluation with Gravity Recovery and Climate Experiment data, *J. Geophys. Res.*, *112*, D07103, doi:10.1029/2006JD007522.

Noborio, K., K. J. McInnes, and J. L. Heilman (1996), Two-dimensional model for water, heat, and solute transport in furrow-irrigated soil: II.

Field evaluation, *Soil Sci. Soc. Am. J.*, *60*(4), 1010–1021, doi:10.2136/sssaj1996.03615995006000040008x.

Oleson, K. W., et al. (2008), Improvements to the Community Land Model and their impact on the hydrological cycle, *J. Geophys. Res.*, *113*, G01021, doi:10.1029/2007JG000563.

Olivella, S., A. Gens, J. Carrera, and E. E. Alonso (1996), Numerical formulation for a simulator (CODE_BRIGHT) for the coupled analysis of saline media, *Eng. Comput.*, *13*(7), 87–112, doi:10.1108/02644409610151575.

Philip, J. R., and V. D. De Vries (1957), Moisture movement in porous materials under temperature gradient, *Eos Trans. AGU*, *38*(2), 222–232.

Pitman, A. J. (2003), The evolution of, and revolution in, land surface schemes designed for climate models, *Int. J. Climatol.*, *23*(5), 479–510, doi:10.1002/joc.893.

Pitman, A. J., et al. (1999), Key results and implications from phase 1(c) of the Project for Intercomparison of Land-Surface Parameterization Schemes, *Clim. Dyn.*, *15*(9), 673–684, doi:10.1007/s003820050309.

Pruess, K. (2004), The TOUGH codes—A family of simulation tools for multiphase flow and transport processes in permeable media, *Vadose Zone J.*, *3*(3), 738–746.

Prunty, L. (2002) Spatial distribution of heat of wetting in porous media, paper 023119 presented at ASAE Annual International Meeting/CIGR XVth World Congress, Chicago, Ill.

Prunty, L., and J. Bell (2007), Infiltration rate vs. gas composition and pressure in soil columns, *Soil Sci. Soc. Am. J.*, *71*(5), 1473–1475, doi:10.2136/sssaj2007.0072N.

Robock, A., C. A. Schlosser, K. Y. Vinnikov, N. A. Speranskaya, J. K. Entin, and S. Qiu (1998), Evaluation of the AMIP soil moisture simulations, *Global Planet. Change*, *19*(1–4), 181–208, doi:10.1016/S0921-8181(98)00047-2.

Rosero, E., Z. L. Yang, L. E. Gulden, G. Y. Niu, and D. J. Gochis (2009), Evaluating enhanced hydrological representations in Noah LSM over transition zones: Implications for model development, *J. Hydrometeorol.*, *10*(3), 600–622, doi:10.1175/2009JHM1029.1.

Rosero, E., Z. L. Yang, T. Wagener, L. E. Gulden, S. Yatheendradas and G. Y. Niu (2010), Quantifying parameter sensitivity, interaction, and transferability in hydrologically enhanced versions of the Noah land surface model over transition zones during the warm season, *J. Geophys. Res.*, *115*, D03106, doi:10.1029/2009JD012035.

Sahimi, M., A. A. Heiba, H. T. Davis, and L. E. Scriven (1986), Dispersion in flow through porous media. II. Two-phase flow, *Chem. Eng. Sci.*, *41*(8), 2123–2136, doi:10.1016/0009-2509(86)87129-9.

Saito, H., J. Šimůnek, and B. P. Mohanty (2006), Numerical analysis of coupled water, vapor, and heat transport in the vadose zone, *Vadose Zone J.*, *5*(2), 784–800.

Scanlon, B. R. (2000), Soil gas movement in unsaturated systems, in *Handbook of Soil Science*, edited by M. E. Sumner, pp. A277–A319, CRC Press, Boca Raton, Fla.

Schrefler, B. A., and X. Y. Zhan (1993), A fully coupled model for water flow and airflow in deformable porous media, *Water Resour. Res.*, *29*(1), 155–167, doi:10.1029/92WR01737.

Schuur, E. A. G., J. G. Vogel, K. G. Crummer, H. Lee, J. O. Sickman, and T. E. Osterkamp (2009), The effect of permafrost thaw on old carbon release and net carbon exchange from tundra, *Nature*, *459*, 556–559, doi:10.1038/nature08031.

Sellers, P. J., et al. (1997), Modeling the exchanges of energy, water, and carbon between continents and the atmosphere, *Science*, *275*(5299), 502–509, doi:10.1126/science.275.5299.502.

Shao, Y., and A. Henderson-Sellers (1996a), Modeling soil moisture: A Project for Intercomparison of Land Surface Parameterization Schemes Phase 2(b), *J. Geophys. Res.*, *101*(D3), 7227–7250, doi:10.1029/95JD03275.

Shao, Y., and A. Henderson-Sellers (1996b), Validation of soil moisture simulation in landsurface parameterisation schemes with HAPEX data, *Global Planet. Change*, *13*(1–4), 11–46, doi:10.1016/0921-8181(95)00038-0.

Šimůnek, J., and M. T. van Genuchten (2008), Modeling nonequilibrium flow and transport processes using HYDRUS, *Vadose Zone J.*, *7*(2), 782–797, doi:10.2136/vzj2007.0074.

Slater, A. G., et al. (2001), The representation of snow in land surface schemes: Results from PILPS 2(d), *J. Hydrometeorol.*, *2*(1), 7–25, doi:10.1175/1525-7541(2001)002<0007:TROSIL>2.0.CO;2.

Thomas, H. R., and M. R. Sansom (1995), Fully coupled analysis of heat, moisture, and air transfer in unsaturated soil, *J. Eng. Mech.*, *121*(3), 392–405, doi:10.1061/(ASCE)0733-9399(1995)121:3(392).

Tillman, F. D., and J. A. Smith (2005), Site characteristics controlling airflow in the shallow unsaturated zone in response to atmospheric pressure changes, *Environ. Eng. Sci.*, *22*(1), 25–37, doi:10.1089/ees.2005.22.25.

Touma, J., and M. Vauclin (1986), Experimental and numerical analysis of two-phase infiltration in a partially saturated soil, *Transp. Porous Media*, *1*(1), 27–55, doi:10.1007/BF01036524.

Twarakavi, N. K. C., J. Šimůnek, and S. Seo (2008), Evaluating interactions between groundwater and vadose zone using the HYDRUS-based flow package for MODFLOW, *Vadose Zone J.*, *7*(2), 757–768, doi:10.2136/vzj2007.0082.

van Dam, J. C., P. Groenendijk, R. F. A. Hendriks, and J. G. Kroes (2008), Advances of modeling water flow in variably saturated soils with SWAP, *Vadose Zone J.*, *7*(2), 640–653, doi:10.2136/vzj2007.0060.

van de Griend, A. A., and M. Owe (1994), Bare soil surface resistance to evaporation by vapor diffusion under semiarid conditions, *Water Resour. Res.*, *30*(2), 181–188, doi:10.1029/93WR02747.

van den Hurk, B. J. J. M., P. Viterbo, A. C. M. Beljaars, and A. K. Betts (2000), Offline validation of the ERA40 surface scheme, *Tech. Memo. 295*, 43 pp., ECMWF, Reading, U. K.

van Genuchten, M. T. (1980), A closed-form equation for predicting the hydraulic conductivity of unsaturated soils, *Soil Sci. Soc. Am. J.*, *44*(5), 892–898, doi:10.2136/sssaj1980.03615995004400050002x.

Walker, J. P., G. R. Willgoose, and J. D. Kalma (2001a), One-dimensional soil moisture profile retrieval by assimilation of near-surface measurements: A simplified soil moisture model and field application, *J. Hydrometeorol.*, *2*(4), 356–373, doi:10.1175/1525-7541(2001)002<0356:ODSMPR>2.0.CO;2.

Walker, J. P., G. R. Willgoose, and J. D. Kalma (2001b), One-dimensional soil moisture profile retrieval by assimilation of near-surface observations: A comparison of retrieval algorithms, *Adv. Water Resour.*, *24*(6), 631–650, doi:10.1016/S0309-1708(00)00043-9.

Wu, Y. S., and P. A. Forsyth (2001), On the selection of primary variables in numerical formulation for modeling multiphase flow in porous media, *J. Contam. Hydrol.*, *48*(3–4), 277–304, doi:10.1016/S0169-7722(00)00180-7.

Zeng, X. B., and M. Decker (2010), Comments on "Improving the numerical simulation of soil moisture-based richards equation for land models with a deep or shallow water table" reply, *J. Hydrometeorol.*, *11*(4), 1051–1054, doi:10.1175/2010JHM1199.1.

Zeng, Y., Z. Su, L. Wan, Z. Yang, T. Zhang, H. Tian, X. Shi, X. Wang, and W. Cao (2009), Diurnal pattern of the drying front in desert and its application for determining the effective infiltration, *Hydrol. Earth Syst. Sci.*, *13*(6), 703–714, doi:10.5194/hess-13-703-2009.

Zeng, Y., Z. Su, L. Wan, and J. Wen (2011), A simulation analysis of advective effect on evaporation using a two-phase heat and mass flow model, *Water Resour. Res.*, doi:10.1029/2011WR010701, in press.

Zhang, C. L., K. P. Krohn, and T. Rothfuchs (2004), Applications of CODE-BRIGHT to thermal-hydromechanical experiments on clays, *Unsaturated Soils: Numer. Theor. Approaches*, *94*, 341–357, doi:10.1007/3-540-26737-9_24.

Z. Su, Faculty of Geo-Information Science and Earth Observation, University of Twente, PO Box 217, NL-7500 AE, Enschede, Netherlands.

L. Wan and Y. Zeng, School of Water Resources and Environment, China University of Geosciences, 100083 Beijing, China. (yijianzeng@gmail.com)

J. Wen, Key Laboratory of Land Surface Process and Climate Change in Cold and Arid Region, Cold and Arid Regions Environmental and Engineering Research Institute, Chinese Academy of Sciences, 320 Donggang West Rd., 730000 Lanzhou, China.